Susanne Reischauer, BSc

Polymerization of Tin Hydrides: Influence of Methods on Material Formation

MASTER'S THESIS

to achieve the university degree of

Diplom-Ingenieurin

Master's degree programme: Advanced Materials Science

submitted to

Graz University of Technology

Supervisor

Univ.-Prof. Dipl.-Chem. Dr.rer.nat., Frank Uhlig

Institute for Inorganic Chemistry

Co-supervisor
Ph.D Ana Torvisco

Graz, Dezember 2018

AFFIDAVIT

I declare that I have authored this thesis independently, that I have not used other than the declared sources/resources, and that I have explicitly indicated all material which has been quoted either literally or by content from the sources used. The text document uploaded to TUGRAZonline is identical to the present master‘s thesis.

Date

Signature

Meinen Eltern, in Dankbarkeit gewidmet!

„Es kommt nicht darauf an, mit dem Kopf durch die Wand zu rennen, sondern mit den Augen die Tür zu finden.“
Werner von Siemens

Danksagung

An dieser Stelle möchte ich mich bei all denjenigen bedanken, die mich während der Anfertigung dieser Masterarbeit unterstützt und motiviert haben.

Mein ganz besonderer Dank gilt meinem Betreuer Frank, für das ermöglichen meiner Masterarbeit und seiner ausgiebigen Unterstützung. Dank deiner herausragenden Expertise konntest du mich immer wieder in meiner Forschung unterstützen. Vielen Dank für Zeit und Mühen, die du in meine Arbeit investiert hast.

Herzlichen Dank gilt Manfred Kriechbaum, der die SAXS-Messungen durchführte. Des Weiteren möchte ich Judith Biedermann für die SEM Messungen danken. Auch Brigitte Bitschnau möchte ich für die Aufnahmen der Pulverspektren einen Dank aussprechen.

Meinen Freunden Laura und Armin, die mich durch mein Studium begleitet haben, danke ich für zahlreiche gemeinsam Lernnachmittage und außeruniversitären Aktivitäten – ohne euch wäre es nur halb so lustig gewesen.

Weiters möchte ich meinem Freund Michi von Herzen danken. Du warst nicht nur privat ein emotionaler Rückhalt für mich, sondern ohne dich und unsere nächtlichen Sn/Ge-Gespräche, wäre meine Arbeit nicht das was sie ist.

Special thank goes to Ana Torvisco. You are not only an incredible teacher, you also became one of my best friends. Thanks for all your great ideas, your support, not only professional, but also personal and your incredible meals in the last years. I will miss you!

Jedoch gilt mein größter Dank meinen Eltern, die mir dieses Studium überhaupt ermöglicht haben und mir mit viel Verständnis und Geduld zu Seite standen. Ihr unterstützt mich in all meinen Entscheidungen und dafür bin ich euch unendlich dankbar.

Danke

Abstract

In the course of this master thesis, the influence of various methods of polymerization on the dehydrogenative coupling reaction of arylSnH$_3$ to aryl decorated nanoparticles (aryl@Sn) has been investigated. This polymerization can be initiated with amine bases, thermally induced using a microwave or *via* an ultrasonication bath.

In order to investigate the influence on the polymerization, *o*-tolylSnH$_3$ and 1-naphSnH$_3$ were used as model substrates and different conditions were employed. All the resulting polymers were investigated by SAXS, WAXS, SEM, XRD, as well as the remaining filtrate of the product was subjected to NMR and GC-MS. Using different concentrations of the amine base TMEDA resulted in slowing down the reaction from around 20 minutes, to almost one hour. Moreover, the slightly larger particles were obtained, due to the extending reaction time. The thermally induced polymerization, a reaction without involving an amine base at room temperature, proceeded quite differently. The reaction time increased from a few minutes to almost two weeks and instead of spherical particles, the macrostructure showed thin stacked-together plates. Interestingly, the structure displayed discrete reflections in the WAXS area corresponding to white tin in the cubic space group I41/amd, which proves the existence of a Sn(0) core in the aryl decorated nanoparticles. In contrast, using a microwave assisted polymerization method without base, the reaction proceeded in a few minutes and the particles showed similar properties that were obtained by a TMEDA induced dehydrogenative coupling reaction. Applying sonication on the polymerization reaction, the bond between Sn-H and Sn-C can be cleaved easier and the particles showed in both cases, with and without an amine base, a more stacked-together nanostructure and an increase of the particle size.

Furthermore, in cooperation with the University in Pardubice, a new synthetic route towards C,N-chelated organotin hydrides, in order to proceed an intra-amine catalyzed dehydrogenative coupling reaction, was established. Therefore, a variety of BX$_3$ protected C,N-chelated organotin halides were able to be isolated and characterized by ^{1}H, ^{11}B, ^{13}C and ^{119}Sn NMR. In addition, two of the obtained compounds were successfully crystallized.

The various methods have a strong influence on the nanostructure, composition and morphology of the formed aryltin decorated tin nanoparticles, which is of high importance for the further use of these materials.

Kurzfassung

Das Ziel dieser Arbeit war es, den Einfluss verschiedener Methoden auf die dehydrierende Kupplungsreaktion von $ArylSnH_3$ zu arylsubstituierten Zinn-Nanopartikel (Aryl@Sn), zu untersuchen. Diese Polymerisation kann durch Aminbasen, thermisch, mit Hilfe von einer Mikrowelle oder durch die Anwendung eines Ultraschallbades, initiiert werden.

Um den Einfluss auf die Polymerisation zu testen, wurden *o*-$tolylSnH_3$ und 1-$naphSnH_3$, als Modelsubstrate verwendet. Die resultierenden Produkte wurden mittels SAXS, WAXS, SEM und XRD untersucht. Des Weiteren wurden NMR und GC-MS Analysen vom Filtrat des Polymeres durchgeführt. Als die dehydrierende Kupplungsreaktion mittels einer geringeren Konzentration der Aminbase TMEDA durchgeführt wurde, konnte die Entstehung von größer Partikel beobachtet werde. Bei Anwendung der thermisch induzierten Methode, ohne einer Aminbase, verlief die Reaktion grundverschieden. Bei der Reaktionszeit handelte es sich nicht mehr um Minuten, sondern um Wochen und anstatt kugelförmiger Partikel, wurden nun aufeinander gestapelte Platten produziert. Außerdem lieferten Reflexe im WAXS Bereich, den Beweis, dass sich im Inneren der Polymere Zinn, in der kubischen Raumgruppe 141/amd, befindet. Im Gegensatz dazu, handelt es sich bei der Reaktionszeit bei einer Polymerisation in der Mikrowelle, um Minuten und es wurden wiederum kugelförmiges Aryl@Sn geformt. Bei der Anwendung von Ultraschall während der dehydrierenden Kupplungreaktion, konnte festgestellt werden, dass die Bildung zwischen Sn-C und Sn-H thermisch labiler ist und daher wurden größere bzw. mehr zusammengewachsene Partikel gebildet.

Des Weiteren wurde, in einer Kooperation mit der Universität in Pardubice, eine neue Syntheseroute, für C,N-chelatgebundenen Organozinnhydride, entwickelt. Dies diente dem Vergleich eines intra- und intermolekularen Katalysators.

Die verschiedenen Methoden haben starke Einflüsse auf die Nanostruktur, die Zusammensetzung und die Morphologie der Polymere und diese Parameter sind von großer Bedeutung für die weitere Verwendung dieser Materialien.

1 Table of Contents

Introduction and Objectives

In the course of this master's work, the dehydrogenative coupling reaction of organotin hydrides to aryl decorated nanoparticles (aryl@Sn) will be investigated. This polymerization can be initiated with amine bases or thermally induced (Figure 1).[1-3] Either the presence of an amine base, which coordinates to the Sn atom or the thermal instability of the organotin hydrides, weaken the Sn-H bond, results in the formation of hydrogen and initialize the dehydrogenative coupling reaction towards the 3D polymeric species.

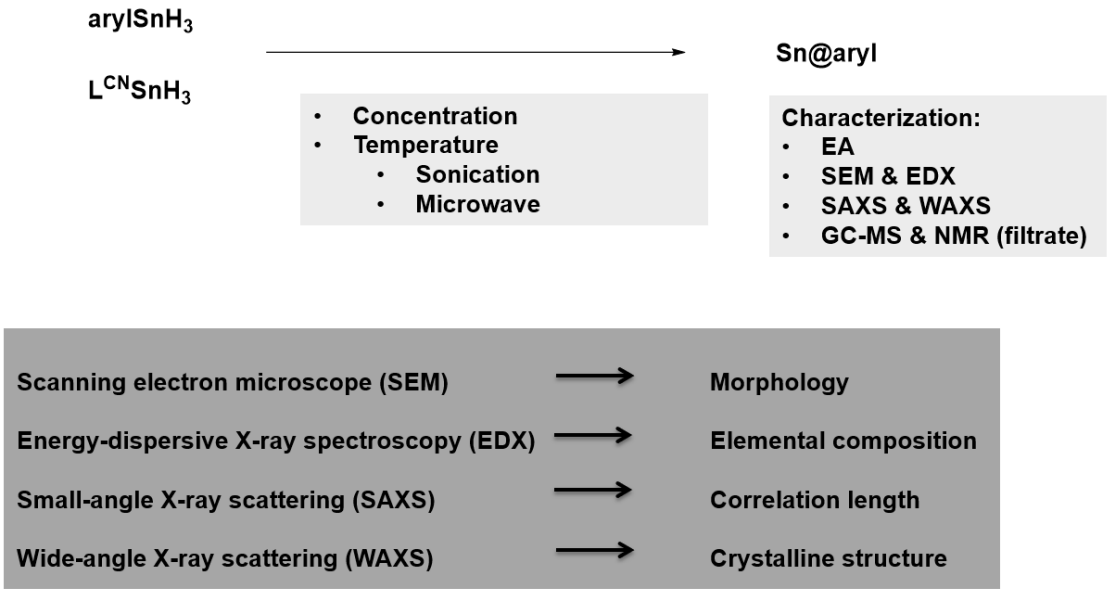

Figure 1: Schematic overview of this work

Different reaction condition will be applied, and the resulting products will be investigated by using SEM, S(W)AXS, NMR (Nuclear Magnetic Resonance), EA and GC-MS (Gas chromatography–mass spectrometry). Due to the fact that the common reaction parameters are always the use of one equivalent of the amine base, the specific concentration influence needs to be studied. Furthermore, because of the thermal instability of the Sn-H bond, the thermally induced dehydrogenative reaction without the direct influence of an amine base will be evaluated. In the course of applying temperature to the organotin hydride,

also the use of a microwave assisted reaction will be investigated. Finally, the influence of ultrasonication waves, in order to introduce vibrations in a molecular level to tin trihydrides, will be explored.

The aim of this project is to accomplish a controlling influence on the nanostructure, composition and morphology of the formed aryl decorated tin nanoparticles, which is of high importance for the further use of these materials.

According to influence of an external amine base on organotin hydrides, it is expected that organotin hydrides exhibiting a L^{CN} moiety are unstable too (Figure 2). It is suggested that these compounds form Sn-Sn bonds without addition of an external amine base. This instability should increase with the number of hydrogens bonded to the tin. Previous attempts at synthesizing organotin trihydrides exhibiting L^{CN} moieties failed because it resulted directly in the conversion towards a polymer. Therefore, this part of the master thesis focuses on the preparation of BX_3 protected C,N- chelated organotin halides, which avoid the N→Sn interaction and function as potential precursors for C,N- chelated organotin hydrides, which can further be used to obtain aryl decorated nanoparticles (aryl@Sn).

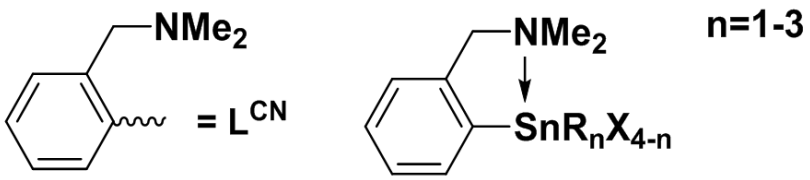

Figure 2: C,N- chelated organotin ligand and N→Sn interaction

2 Theoretical Background

Since 3500 BC, tin has been known as a metal and was a highly appreciated raw material for further processing. The first organotin compound was synthesized by Frankland by heating iodoethane in the presence of metallic tin (Scheme 1).[4, 5]

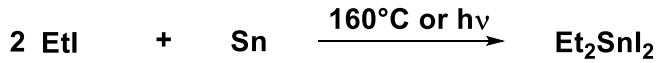

Scheme 1: Synthesis of the first organotin compound by Frankland

In 1900, Grignard discovered the synthesis of organomagnesium halides in ether solution.[6] This opened a new synthetic route for organostannanes, replacing Frankland's route, because it was less sensitive than his indirect method. The most popular method to generate tetrasubstituted organostannanes is the reaction of a Grignard reagent with tin halides in solvents such as tetrahydrofuran (THF) or diethyl ether (Et_2O) (Scheme 2).[7-11]

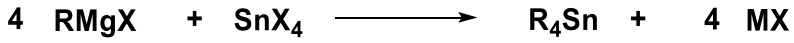

Scheme 2: General reaction of a Grignard reagent with a tin halide

Another well-known method in order to obtain tetraarylstannanes is the lithiation of organohalides followed by a treatment with SnX_4.[12] For the next step towards monoorganotin trihalides the Kozeshkov reaction is usually the method of choice. Kozeshkov described the first solvent free preparation of $RSnX_3$ compounds (Scheme 3).[13-16] In accordance to monoorganotin trihalides, it is also possible to synthesize di- and triorganotin halides.[7, 17]

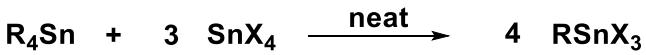

Scheme 3: Kozeshkov reaction to synthesize monoorganotin trihalides

In contrast to organotin halides, the challenge concerning the preparation of tin hydrides is the fact that they are oxygen and temperature sensitive. This is due to the low dissociation energy of the metal hydride bond.[18] The first stannane, SnH_4 (tin tetrahydride), was described by Paneth and his co-workers in 1920.[19] Two years later, Kraus and Greer synthesized and characterized $(CH_3)_3SnH$ (trimethylstannane) (Scheme 4).[20] In the following years, further tin hydrides using this method were published.[21-23]

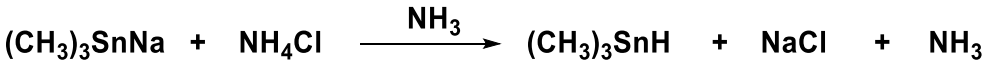

Scheme 4: Synthetic route published by Kraus and Greer

Finholt developed in 1947 a newer and more convenient route in which lithium aluminium hydride ($LiAlH_4$) reduces organotin chlorides in order to obtain the corresponding hydrides.[24] This preparation method is until today the method of choice to synthesize organotin mono-, di- and trihydrides.[25, 26] In 2013, the working group of Uhlig published the synthesis of several aryltin trihydrides ($ArSnH_3$), which were used as educts in this master thesis (Scheme 5).[26]

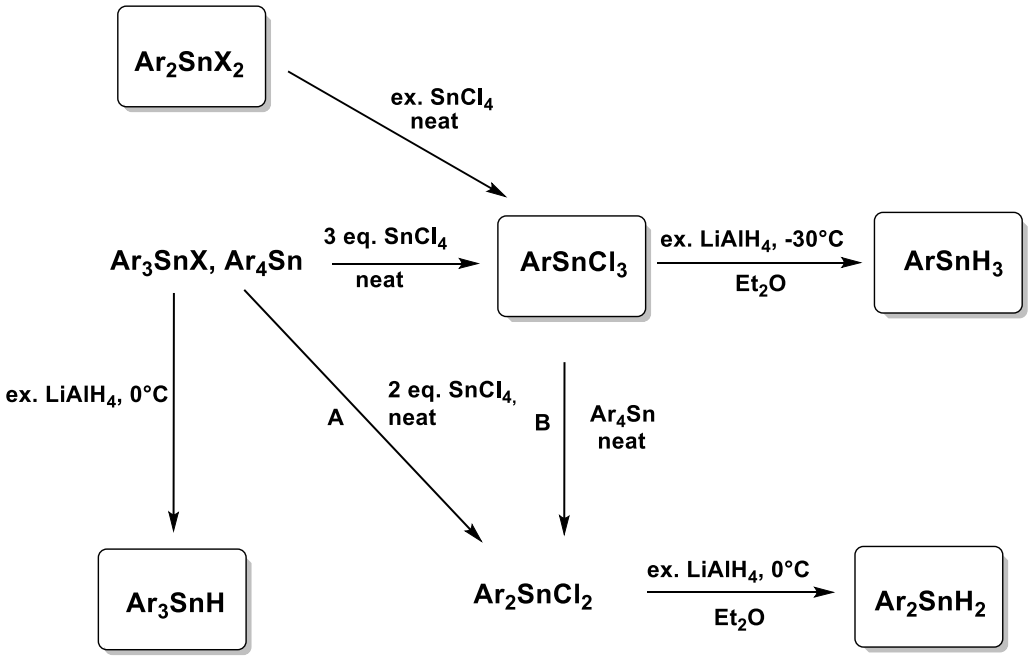

Scheme 5: General synthetic routes towards aryltin monohydrides (Ar_3SnH), aryltin dihydrides (Ar_2SnH_2) and trihydrides ($ArSnH_3$)[26]

2.1 Linear Polystannanes

Over the years, tin polymers have reached higher interest due to their variety of possible applications. Linear polystannanes are describe with the formula $(R_2Sn)_n$ and they can be visualized as a covalently linked metal backbone which is surrounded by an organic jacket (Figure 3).[3, 27-40]

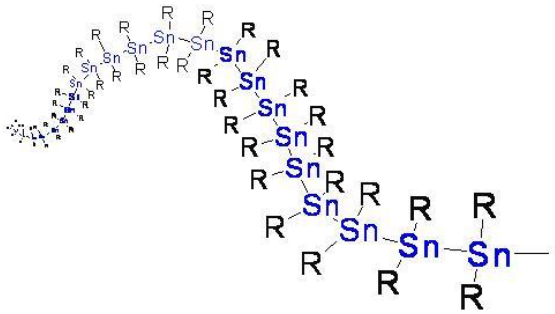

Figure 3: Schematic of a linear polystannane

With increasing number of covalent Sn–Sn bonds, the delocalization of σ-electrons along the backbone transforms discrete frontier orbitals into a σ-σ* band structure (σ-conjugation)[41-44] with strong σ-σ* transitions.[42, 45-56] This is also the reason for the characteristic yellow or orange color and the UV absorptions in the region of 375-410 nm.[57-59] These compounds have a very low band gap which could be minimized by adding aromatic groups as a residue, because they would lead to σ-π delocalization.[41, 42] For all these reasons, the linear polystannanes are a highly conductive metallic material and therefore, are very promising compounds for applications in electronic devices, charge transport, non-linear optical materials and many more.[42, 46, 50, 52, 54, 56, 60-64]

2.1.1 Organotin Dihydrides Towards Linear Stannanes

2.1.1.1 Wurtz-Type Coupling

As already mentioned above, Löwig was the first one who published the synthesis of oligo- and polystannanes in 1852 by reacting ethyl iodide with tin/sodium.[65] By heating iodoethane with metallic tin and sodium, Cahours[66, 67] generated a compound with an elemental composition that matched the formula $(SnEt_2)_n$. Furthermore, he tried to obtain poly(dimethylstannanes), but he had problems to prove his results until Price repeated his reaction and confirmed his claim.[46] Since then, Cahours is known as the pioneer of the Wurtz-type reaction. By applying the reaction with sodium in organic solvents such as toluene, many poly(alkylstannanes) were synthesized, although oligostannanes and cyclic products were

produced as side products (Scheme 6).[59, 65, 68-71] Caseri *et al.* published in 2011 a modified Wurtz-type reaction by using sodium in liquid ammonia to obtain polymers.[54]

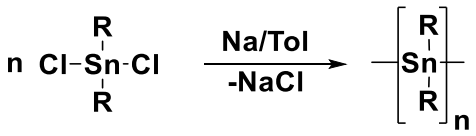

Scheme 6: Wurtz-type coupling for the preparation of polystannanes

2.1.1.2 Solvent- and Catalyst free Dehydrogenation

Foucher and his co-workers published in 2010 the successful synthesis of oligo- and polystannanes *via* thermal induced dehydrocoupling in the absence of an amine base such as TMEDA, pyridine or DMAP. (Scheme 7).[72]

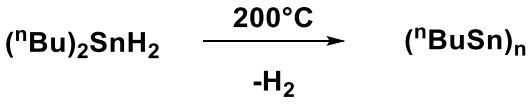

Scheme 7: Thermal hydrocoupling of dibuthyltin dihydride

2.1.1.3 Metal Catalyzed Dehydrogenation

The most common route to synthesize chain polymers out of organotin dihydrides is the catalytic dehydrogenation using transition metal and lanthanide complexes (Scheme 8).[42, 45, 48-51, 53, 57, 59, 60, 73-82]

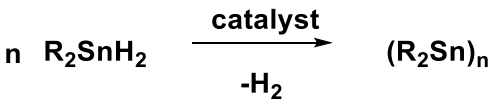

Scheme 8: Metal catalyzed dehydrogenation reaction producing linear stannanes

By using this synthetic route, a variety of polystannanes were produced. Choffat *et al.* reported the synthesis of poly- and distannanes using a lanthanide diamide based catalyst.[76] Furthermore, Beckmann *et al.* were able to generate chiral linear stannanes by mixing the starting chlorides with a Wilkonson's catalyst.[83] The working group of Foucher published recently asymmetrical hyperconjugated polystannanes, partly inserted alkene tin polymers and also polybis(dimethylstannanyl)ferrocene.[84-86]

2.1.1.4 Condensation

Sommer *et al.*[87] and Uhlig *et al.*[88] have published a route which can be used to synthesize cyclostannanes, as well as oligostannanes. Foucher was able to develop a new synthetic protocol in order to generate alternating polystannanes which involves the condensation of organotin dihydrides with organotin diamides in toluene or diethyl ether (Scheme 9).[32, 87]

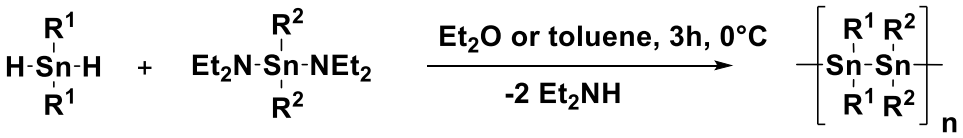

Scheme 9: Preparation of polystannanes *via* condensation

To enhance light stability and solubility this method can be used to synthesize a product which has both, diaryl and dialkyl substituents included.[32, 41]

2.1.1.5 Electrochemical Synthesis

Another way to synthesize polystannanes, without further compounds involved, is the electrochemical pathway. Diorgano dihalides are reduced in a one-compartment cell, where platinum is used as a cathode and silver as an anode. The solvent is always 1,2-dimethoxyethane and as a supporting electrolyte tetrabutylammonium is needed (Scheme 10).[52, 89]

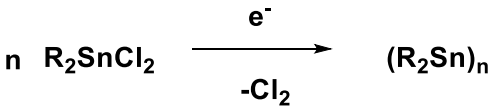

Scheme 10: Electrochemical route to synthesize linear polystannanes

2.1.1.6 Dehydrogenative Coupling Using an Amine Base

Neumann was the first who described the formation of Sn-Sn bonds using a nitrogen base as a catalyst.[90, 91] Davies[92] and Mathiasch[93] applied the method successfully in order to produce distannanes from tin hydrides. There are two mechanisms suggested for the formation of Sn-Sn bonds either *via* a polar process or a radical formation.[94, 95] The polar process would occur by a formation of a four membered transition state and the radical

mechanism would form a $R_3Sn\cdot$ radical which would replace a hydrogen atom. This would lead to the production of molecular hydrogen by generating more and more Sn-Sn bonds. In 2011, Uhlig and his co-workers published the use of the amine base TMEDA (*N,N,N',N'*-tetramethylethylenediamine) to synthesize poly(dialkylstannane)s and poly(diarylstannane)s (Scheme 11).[96]

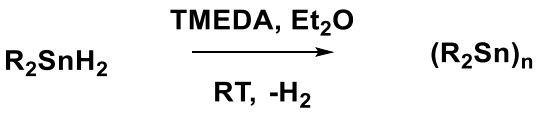

Scheme 11: General dehydrogenation using TMEDA as an amine base

2.2 3D Polymers *via* Amine Catalyzed Dehydrogenative Coupling of Tin Trihydrides

Recently, Sindlinger and his co-workers published the dehydrogenative coupling reaction of Ar*SnH_3 (Ar*= 2,6-trip$_2$(C_6H_3), trip= 2,4,6-triisopropylphenyl) using amine bases such as DMAP (4-dimethylaminopyridine), pyridine and TMEDA. They successfully isolated the diorganodistannane, Ar*H_2Sn–SnH_2Ar*, by using a catalytic amount of the amine base. By applying an excess of pyridine, the thermally stable monomeric base adduct Ar*SnH was generated. Due to their highly sterically encumbered aryl group, they never observed a higher molecular Sn compound.[97, 98]

In contrast to the well-studied linear polystannanes, the dehydropolymerization of monoorganotin trihydrides had been neglect so far. Recently, Uhlig *et al.* reported the dehydrogenation of several tin trihydride species ($RSnH_3$) adding TMEDA in order to afford 3D polystannanes, also described as aryl decorated nanoparticles (Sn@aryl). The well-studied reaction is the TMEDA induced dehydrogenated coupling of *o*-tolylSnH_3, which shows a distinct color change from colorless, which is specific for Sn(IV) compounds, over yellow, consistent with tin in an oxidation state II, towards black, suggesting formation of Sn(0). In contrast to the linear polymers, the remaining Sn-H bond allows to form a 3D structure, by removing hydrogen and the cleavage of Sn-C(aryl) groups (Scheme 12). The black polymeric material is not soluble in any organic solvent and therefore does not allow standard characterization methods such as ^{1}H, ^{13}C, ^{119}Sn NMR, GC-MS or GPC. According to GC-MS and NMR measurements of the remaining filtrate, toluene was detected when using *o*-tolylSnH_3, which proves the claim of Sn-C cleavage.

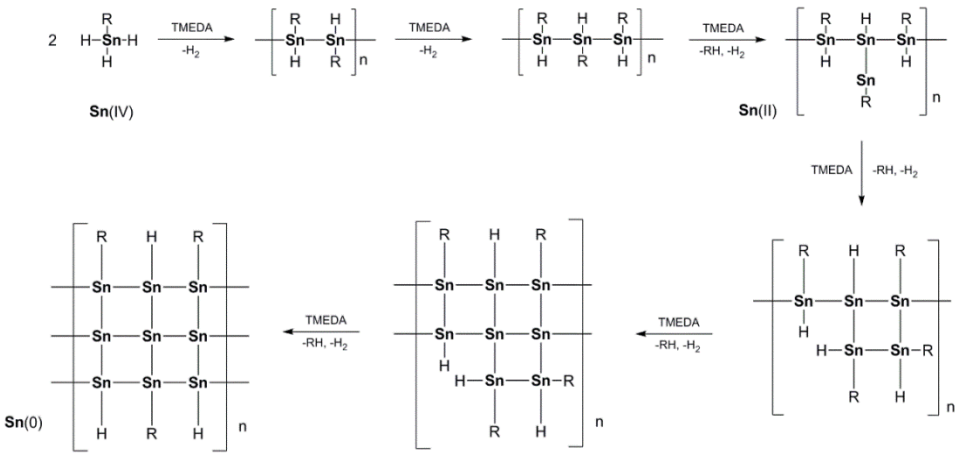

Scheme 12: Suggested mechanism of the dehydrogenative coupling reaction of monooragnotri trihydrides

SEM (Scanning Electron Microscope) images show particles with a spherical morphology, with a diameter of 1 µm. But with increasing magnification, it is shown that the particles consist of smaller units with a spherical nature and a size range of 7-30 nm (Figure 4).

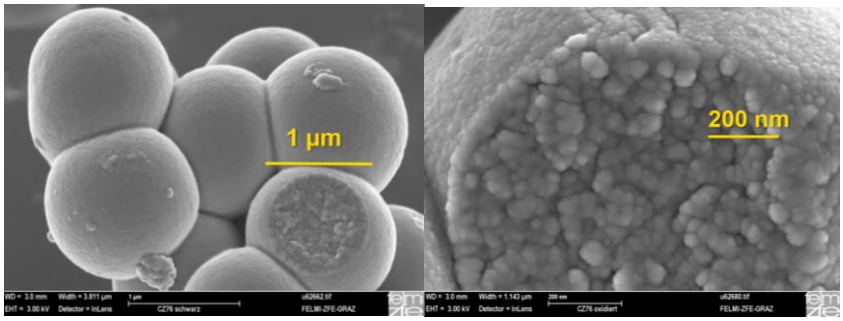

Figure 4: FESEM (field emission SEM) images of the polymeric material Sn @*o*-tolyl

In situ SAXS measurements at several Synchrotrons (Grenobel, Triest) also confirmed the claimed formation of a superstructure in the first few minutes and then agglomeration to larger spherical particles. Moreover, TEM (Transmission electron microscopy) measurements confirmed the organic core shell structure in which the metal tin (0) core is embedded.[1, 2]

3 Results and Discussion

3.1 Amine Concentration Dependent Dehydrogenative Polymerization

Neumann was the first who described the formation of Sn-Sn bonds using a nitrogen base as a catalyst.[90, 91] Davies[92] and Mathiasch[93] applied the method successfully in order to produce distannanes from tin monohydrides. Since then, using amine bases, such as TMEDA, pyridine, piperidine, diethylamine and dimethylformamide, has become quite rare in preparation of Sn-Sn bonds.[87, 90, 91] But in 2011, Uhlig and his co-workers published the TMEDA catalyzed synthesis of linear polystannanes and since then more and more methods producing these 2D polymers came up.[96] However, Neumann published many suggestions and observations, such as the formation upon hydrogen evolution, but an exact knowledge about the mechanisms of the formation of the Sn-Sn bond has not been known so far.[99] Sindlinger also suggested a mechanism for the amine catalysed dehydrogenation of highly sterically encumbered aryltin trihydrides using pyridine and DMAP (4-dimethylaminopyridine) in a catalytic amount, but still the exact role of the amine base was not clear.[97] This was the motivation for Uhlig and his working group to investigate the TMEDA induced dehydrogenation of *o*-tolylSnH$_3$ (**6**) in more detail. It was found that the amine base coordinates to the Sn atom, therefore the Sn-H bond elongates, and this initializes the dehydrogenative coupling. In contrast to linear polystannanes, the introduction of a further reaction site leads to the remaining presence of a Sn-H compound which allows the formation of a 3D polymer by removing hydrogen and the cleavage of Sn-C(aryl) groups. The yielded black polymeric material is not soluble in any common solvents and therefore does not allow standard characterization methods such as NMR, GC-MS or GPC.[1] Since the reaction mechanism is well investigated, the parameters which influence the dehydrogenative coupling reaction need to be studied in order to be able to tune the size, shape and composition of the nanoparticles, which are key to synthesizing a possible high capacity substitute for the graphite anode of lithium ion batteries.

3.1.1 Reaction of Aryltin Trihydrides with Different Concentrations of TMEDA

Within this work the synthesis of the educt *o*-tolylSnH$_3$ (**6**) was carried out *via* the literature known procedure; by the hydrogenation of the starting material *o*-tolylSnCl$_3$ (**4**) with LiAlH$_4$ at -30°C.[26] The common reaction conditions for the dehydrogenative coupling of organotin trihydrides, are Et$_2$O as a solvent and 1 eq. TMEDA as an amine base at room temperature in order to obtain Sn@$^{1\text{ eq. TMEDA}}$*o*-tolyl (**12**) (Scheme 6).

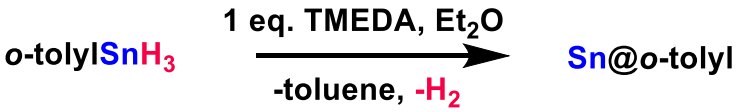

Scheme 6: Polymerization of o-tolylSnH$_3$ (**6**) with 1 eq. TMEDA

After the addition of TMEDA, a distinct color change, from colorless Sn (IV), to a yellow/orange species, indicating Sn in the oxidation state II, towards a black precipitate which contains of Sn (0) nanoparticles, proceeds (Figure 5).

Figure 5: Color change of the reaction Sn@$^{1\text{ eq. TMEDA}}$*o*-tolyl (**12**)

The reaction time to synthesize **12** took about 20-30 minutes. To get information about the influence of the concentration of the amine base, a reaction with 0.1 eq. of TMEDA was performed. As expected, the dehydrogenative coupling reaction towards the aryl decorated particles Sn@$^{0.1\text{ eq. TMEDA}}$*o*-tolyl (**13**) took longer, namely 45 minutes to complete. The isolated powders Sn@$^{1\text{ eq. TMEDA}}$*o*-tolyl (**12**) and Sn@$^{0.1\text{ eq. TMEDA}}$*o*-tolyl (**13**) were studied with SAXS to get information about the correlation length in the nanoscale region. A slight difference in correlation length from 1.86 nm (**12**) to 1.80 nm (**13**) was detected in the measurement (Figure 6). In contrast to later shown polymers, both **12** and **13** did not generate any reflections in the WAXS area, which could be assigned to planes belonging to white tin. Furthermore, the morphology was investigated by SEM to observe any appreciable change in the nanostructure. The reaction performed with less amine base (**13**) led to the formation of larger particles. Due to the extended reaction time, the particles have more time to

agglomerate and form this specific structure (Figure 7). The loss of the organic group toluene was proven by GC-MS and EA in both reactions. In summary, with the reduction of the concentration of the amine base, the size of the spherical particles can be tuned, while the other parameters, such as elemental composition and shape, stay the same.

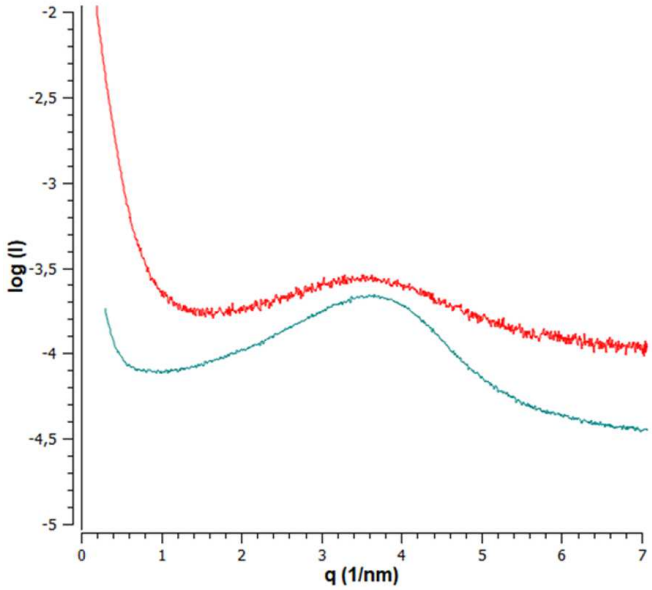

Figure 6: SAXS measurements of Sn@$^{1\text{ eq. TMEDA}}$*o*-tolyl (**12**) (blue) and Sn@$^{0.1\text{ eq. TMEDA}}$*o*-tolyl (**13**) (red)

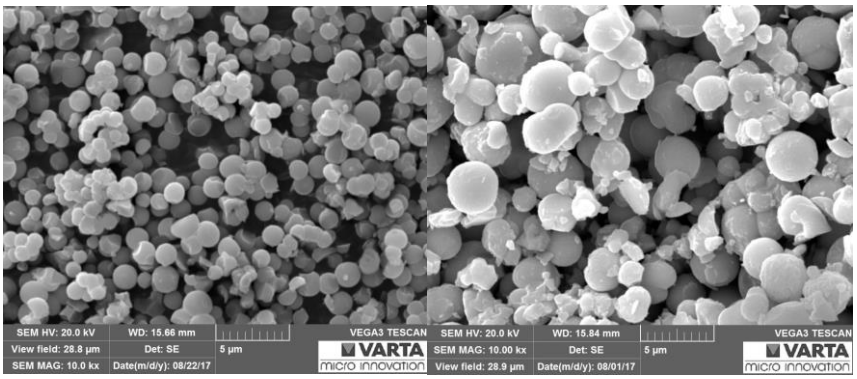

Figure 7: Comparison of SEM images of the polymers formed Sn@$^{1\text{ eq. TMEDA}}$*o*-tolyl (RT, 20 min) (**12**) (left) and Sn@$^{0.1\text{ eq. TMEDA}}$*o*-tolyl (RT, 45 min) (**13**) (right)

3.2 Temperature Induced Dehydrogenative Coupling

Higher group 14 metal hydrides have a distinct sensitivity towards oxygen and temperature. The reason for this behavior is the rather low dissociation energy of the metal-hydrogen bond.[100] The stannane (SnH_4), as well as most organotin hydrides undergo rapid decomposition at room temperature under formation of hydrogen and elemental tin (Scheme 7).[101] This distinct temperature sensitivity can be decreased by the substitution of hydrogen atoms with an alkyl or aryl moiety. Moreover, the stability of alkyl compounds are increased by the size of the substituents.[102]

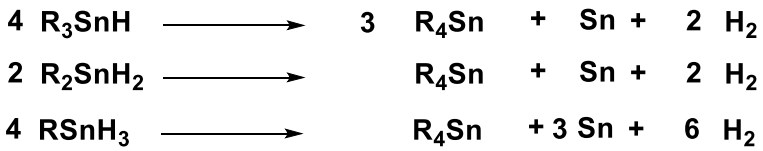

Scheme 7: Decomposition of organotin hydrides

Foucher and his co-workers utilized the temperature sensitivity of organotin dihydrides and successfully synthesised oligo- and polystannanes *via* thermal induced dehydrocoupling.[72] This is also the motivation for this master thesis: to exploit the instability of the Sn-H bond in order to obtain a polymer by thermally induced dehydrogenative coupling under a variety of conditions.

3.2.1 Thermally Induced Polymerization of Aryltin Trihydrides

Due to the absence of an amine base, the thermally induced polymerization is a much slower reaction, which gives the opportunity to study the reaction mechanism closer. The mechanism of the dehydrogenative coupling reaction of organotin trihydride has already been calculated in our working group by DFT- calculations (Scheme 8) and confirmed by EXAFs (Extended X-Ray Absorption Fine Structure) and XANES (X-ray Absorption Near Edge Structure). A former student was able to observe the intermediate B by applying 80°C and vacuum for about 20 minutes to *o*-tolylSnH$_3$ (**6**).[1] The proton NMR of H$_2$[(*o*-tolyl)Sn–Sn(*o*-tolyl)]H$_2$ (**10**) could be nicely compared to already published similar compounds from the Sindlinger[97] working group. All attempts to crystallize **10** in various solvent combinations failed.

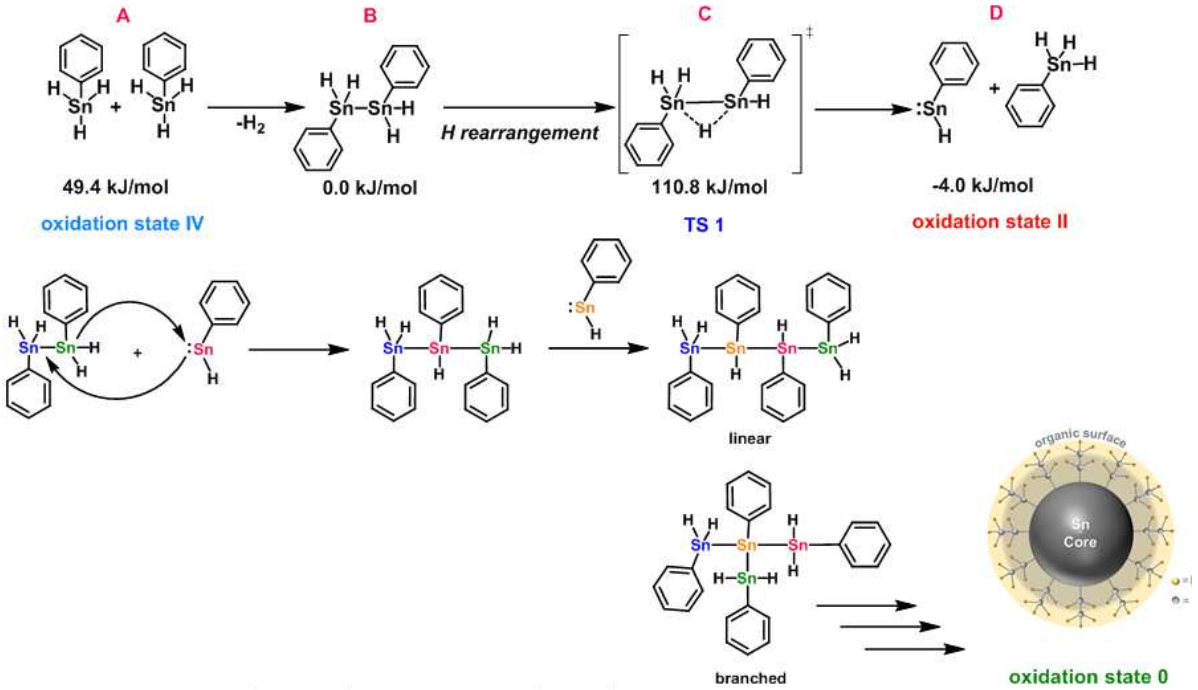

Scheme 8: Suggested mechanism for the dehydrogenative coupling reaction of aryltin trihydrides

With the motivation of stabilizing the distannane intermediate, larger aryl residues were employed in course of this master thesis. Firstly, 2,4,6-mesSnH$_3$ (**7**) was used to perform the reaction, but as the educt is a solid the polymerization performed much faster and there was no sign of the intermediate, although low temperature NMR experiments were performed to lower the reaction speed of the dehydrogenation coupling reaction. Next, the thermally induced reaction was done with 1-naphSnH$_3$ (**8**) as a substrate. Here a lot of problems came up, concerning the aryl cleavage, due to the fact the naphthalene is a solid and cannot be removed as easily as it was the case with toluene. Due to these drawbacks, focus was placed on slightly less stable aryl residues and therefore PhSnH$_3$ (**9**) was treated with 40°C under vacuum. The proton shifts, as well as the coupling constants, which are illustrated by dotted lines, of the synthesized intermediate H$_2$[PhSn–SnPh]H$_2$ (**11**) fit to the already known H$_2$[*o*-tolylSn–Sn*o*-tolyl]H$_2$ (**10**) (Figure 8). Both ^{1}H spectra show the hydride peak around 5 ppm and the values for coupling constants of the known **10** compound, which are $^1J(^{119}\text{Sn-}^1\text{H})$ = 1734 Hz and $^1J(^{117}\text{Sn-}^1\text{H})$ = 1656 Hz, compares well to the couplings of **11** ($^1J(^{119}\text{Sn-}^1\text{H})$ = 1758 Hz and $^1J(^{117}\text{Sn-}^1\text{H})$ = 1677 Hz). In the ^{119}Sn spectrum, the shift of H$_2$[(*o*-tolyl)Sn–Sn(*o*-tolyl)]H$_2$ (**10**) is at -353.9 ppm (^1J ($^{119}\text{Sn-}^1\text{H}$) = 1763 Hz, $^2J(^1\text{H-}^{119}\text{Sn})$ = 150 Hz), which can again be well compared to **11**, where the shift is found at -370.7 ppm (^1J ($^{119}\text{Sn-}^1\text{H}$) = 1734 Hz, $^2J(^1\text{H-}^{119}\text{Sn})$ = 135 Hz).

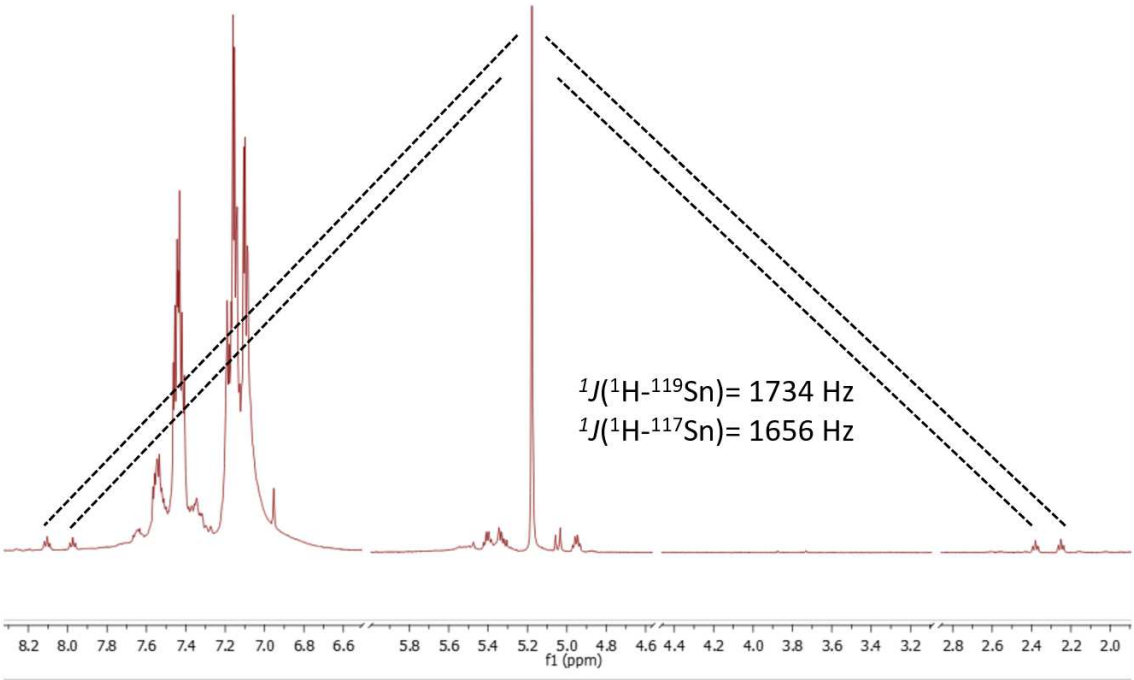

Figure 8: Section of the ^1H spectrum of $H_2[PhSn–SnPh]H_2$ (**11**)

Due to successful experiments concerning the intermediates, the thermally induced dehydrogenative coupling towards Sn@*o*-tolyl (RT, 16 days) (**14**) was also investigated (Scheme 9). This reaction proceeded much slower than the amine induced polymerization. The formation of polymer **14** took about 2 weeks to be completed.

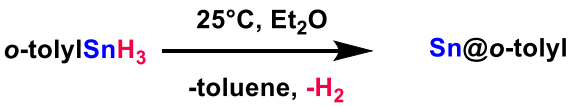

Scheme 9: Thermally induced polymerization of **14**

The formed polymeric material **14** was investigated by SAXS, as well as WAXS measurements in order to determine information concerning the correlation length and the crystalline structure (Figure 9). However, while, no correlation length was observed in the SAXS region, in the WAXS spectrum discrete reflections, which could be assigned to the 2/0/0 and 1/0/1 planes of white tin in cubic space group 141/amd, were detected. This proved the suggested model of the polymer containing a Sn core which is surrounded by an organic surface (Figure 10).

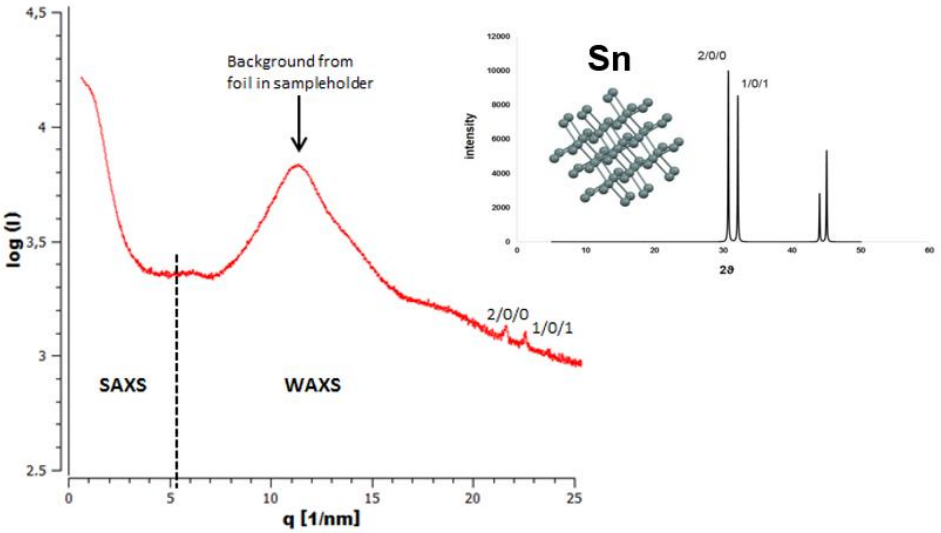

Figure 9: SAXS and WAXS measurement of the thermal induced dehydrogenative coupling product **14**

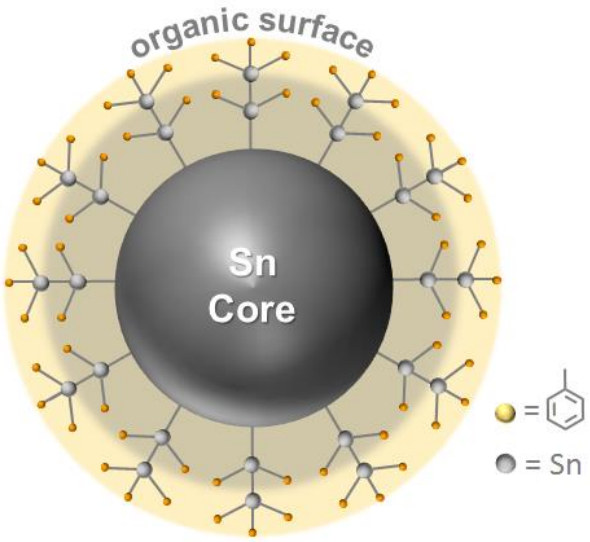

Figure 10: Suggested model of the Sn@aryl polymer

Furthermore, SEM images of Sn@*o*-tolyl (**14**) were recorded in order to reveal the morphology differences on a µm scale. In contrast, to the spherical particles in Sn@$^{1\ eq.\ TMEDA}$*o*-tolyl (**12**) and Sn@$^{0.1\ eq.\ TMEDA}$*o*-tolyl (**13**), we know from the amine catalyzed polymerization, the shape looked very different. Due to the longer reaction speed, the microstructure of **14** is more organized, as the WAXS measurement proved, but the macrostructure lost the spherical morphology. The thermally induced polymerization product **14** looked more like plates which were stacked-together over time (Figure 11).

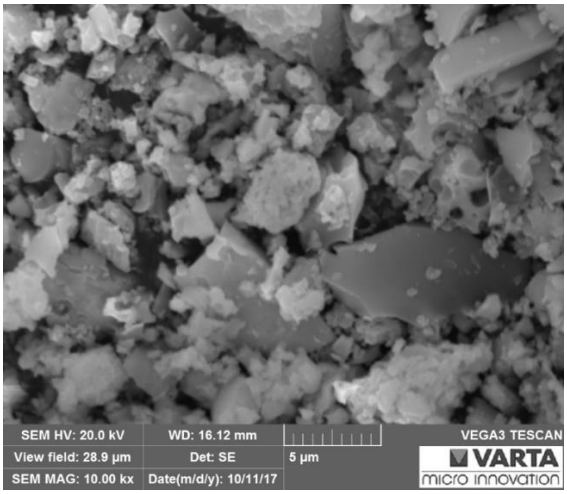

Figure 11: SEM image of the thermal induced polymerization product **14**

In conclusion, the thermal conversion of sterically less demanding aryltin trihydrides led to observation of an intermediate during the polymerization reaction, as well as peaks within WAXS measurements, which proved the suggested model. Furthermore, by increasing the reaction time also a complete different morphology was obtained.

3.3 Sonication Assisted Dehydrogenative Polymerization

In the last century the field of synthesizing nanoparticles with the assistance of sonication has become a growing field. In 1996, Suslick was one of the first who published the application of ultrasonication to generate nanostructured materials and thus pioneered the use of this method in material science.[103, 104] Since then, a huge amount of publications, dedicated to the synthesis of various nanoparticles with the help of sonication, came up, however, not in the field of tin hydrides.

Sonication uses sound waves to distribute particles in a solution through the conversation of electrical signals into physical vibrations. Bubble collapses in the solvent result in harsh concentrations of energy, which generate high local temperatures and pressure. Combining these conditions with rapid cooling, these are unique extreme conditions for driving chemical reactions.

3.3.1 Influence of Ultrasonication on the Polymerization of Aryltin Hydrides

In order to understand the influence of sonication on dehydrogenative coupling, a reaction with and without the amine base TMEDA under cooling at room temperature was proceeded. The thermally induced sonication assisted polymerization of *o*-tolylSnH$_3$ (**6**) towards Sn@^{son}*o*-tolyl (RT, 20 days) (**15**) showed only a slight difference in the reaction time to the thermal induced polymerization without sonication Sn@*o*-tolyl (RT, 16 days) (**14**). Having a closer look at the morphology, SEM images were recorded and showed, in contrast to **14**, particles which are stacked more closely. Furthermore, SAXS measurement resulted in no correlation length due to the fact that the macrostructure is not organized at all. Contrary, the WAXS spectrum displayed again reflections which can be assigned to the planes of white tin (Scheme 10).

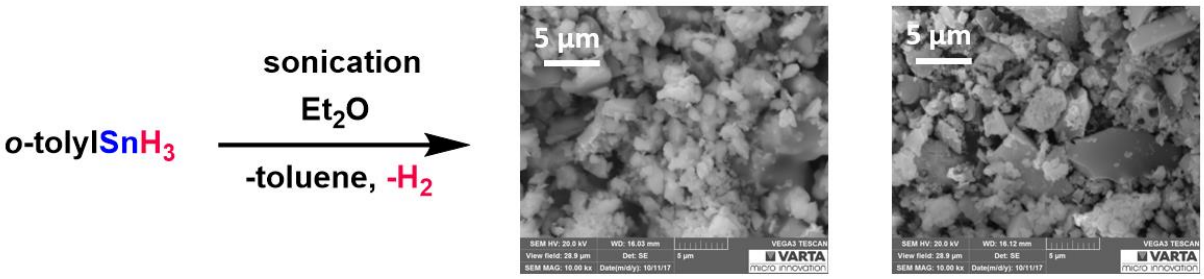

Scheme 10: Sonication reaction towards Sn@$^{son.}$*o*-tolyl (RT, 20 days) (**15**) (left) and the comparison to **14** (right)

The additional amine induced sonication assisted polymerization towards Sn@$^{son,\ 1\ eq.\ TMEDA}$*o*-tolyl (RT, 30 min) (**16**) showed the same phenomena as the reaction above. The synthesized particles **16**, which have a spherical shape, due to the presence of TMEDA, are larger and more agglomerated as in the experiment without sonication **12** (Scheme 11).

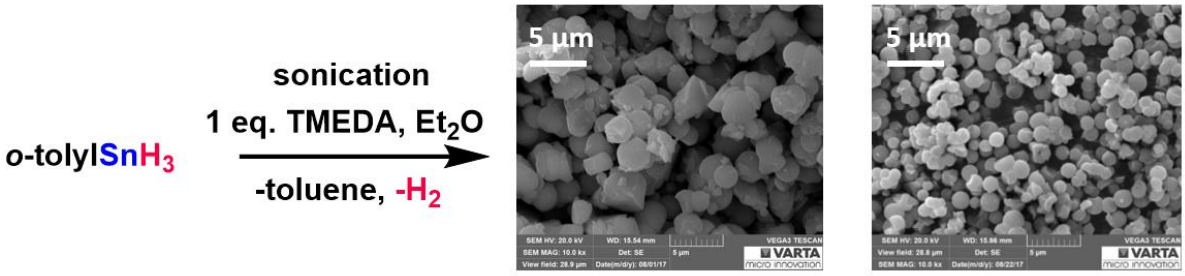

Scheme 11: Sonication reaction towards Sn@$^{son,\ 1\ eq.\ TMEDA}$*o*-tolyl (16) (left) and the comparison to Sn@$^{1\ eq.\ TMEDA}$*o*-tolyl (**12**) (right)

To investigate if the already synthesized polymer Sn@$^{1\ eq.\ TMEDA}$*o*-tolyl (**12**) can be changed in respect to morphology or nanostructure by sonication, **12** was also treated with this method. For the first experiment, **12** was exposed to sonication waves for 24 hours and the SEM images showed a morphology change to more stacked-together particles, as already seen above. By extending the exposure to 4 days, the phenomena continuous, and the spherical particles grow very close together (Scheme 12). Also, GC-MS and NMR measurements of the filtrate prove the loss of the organic leaving group toluene.

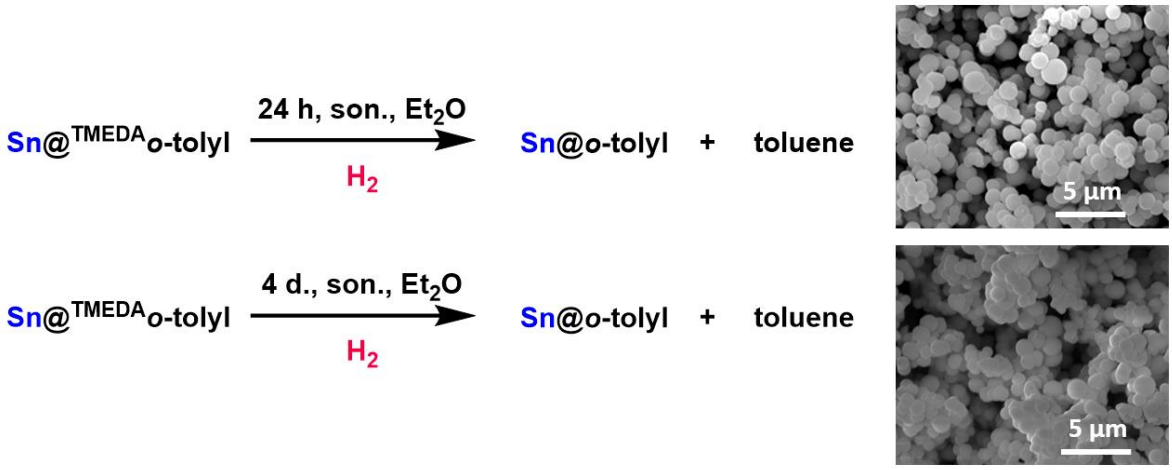

Scheme 12: Sonication of Sn@$^{1\ eq.\ TMEDA}$*o*-tolyl (RT, 20 min) (**12**) for 24 h and 4 days

Due to this fact, it is suggested, that due to the vibration of the sonication, the bond between remaining Sn-H and Sn-C can be cleaved easier and therefore parts of the organic surface are removed in order to generate new active sites, where the particles can grow further through Sn-Sn bond formation (Figure 12).

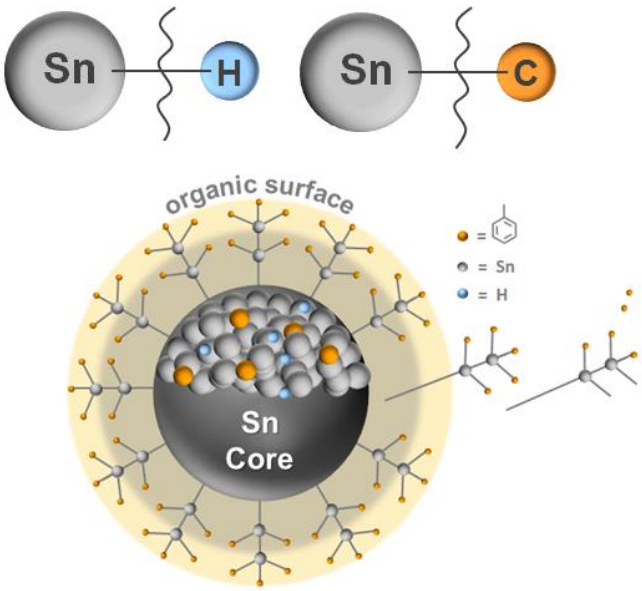

Figure 12: Suggested model for sonication experiments

3.4 3D Polymers of Group 14 Elements

One of the main goals of our working group is the synthesis of group 14 3D polymers (Scheme 13). The big advantages of germanium and tin atoms, is to induce metallic character into the polymeric material, which can be very useful for their future applications.[40, 46, 55, 134-139] Such materials are highly conductive and could be promising for applications in non-linear optical materials, photoresists in microlithography, charge-transport, doping of semiconductors and electronic devices.[42, 46, 50, 52, 54, 56, 60-64, 105, 106] As with organotin trihydrides, the synthesis of 3D polymers was already successful, it was inevitable to expand the focus to other group 14 metals. First attempts synthesizing silicon 3D polymers were not successful, however converting organogermanium trihydride towards aryl decorated nanoparticles using amine bases and conventional heating (reflux) worked resulting in very low yields. Therefore, stronger reaction conditions than using TMEDA at room temperature, such as an amine catalyzed microwave assisted method, was established to form polymeric material. In order to compare the 3D polymers, the same method was applied to organotin trihydrides.

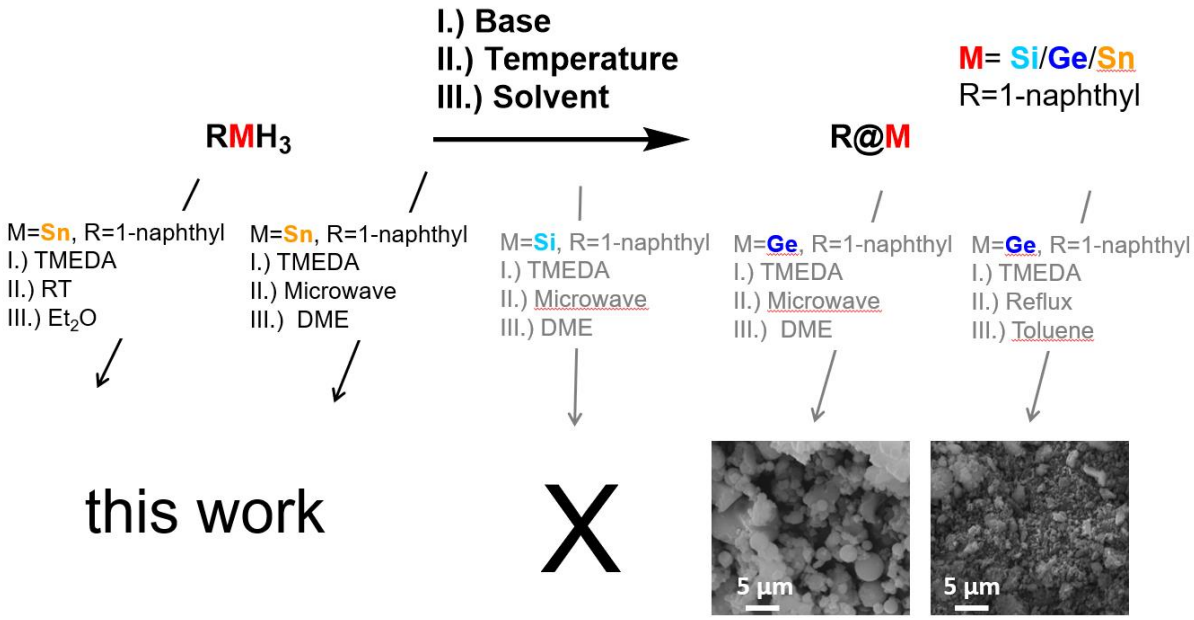

Scheme 13: Comparison of group 14 3D polymers

3.4.1 Microwave Assisted Polymerization of Aryltin Trihydrides

To only observe the influence of the metal in the polymer, other reaction variables including the residue and the solvent were kept the same. The first attempt synthesizing Sn@^{micro}1-naphthyl (**17**) by applying 100°C for 20 minutes resulted in a dark grey powder, which was subjected to SAXS, WAXS, SEM and EA (Scheme 14).

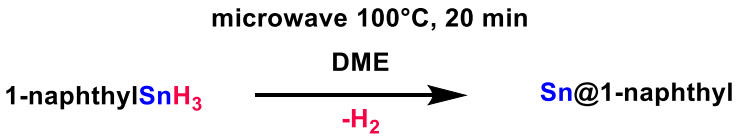

Scheme 14: Synthesis of Sn@^{micro}1-naphthyl (**17**)

The SAXS spectra showed not only reflections which could be assigned to white tin, as mentioned above, but also other peaks, which could be related to agglomerations of the leaving group naphthalene, were observed (Figure 13). This suggests that, due to the strong polymerization method, the leaving group was cleaved, but not removed from the polymeric material. In addition, the SEM image confirmed this suggestion. It seemed like rods, which only consist of carbon and hydrogen, incooperated in Sn@^{micro}1-naphthyl (**17**) (Figure 14). Attempts to remove all of the naphthalene by washing with various solvents such as DME, hexane, pentane, THF and toluene failed, due to the fact that the organic residue is directly inserted in the structure of the polymer.

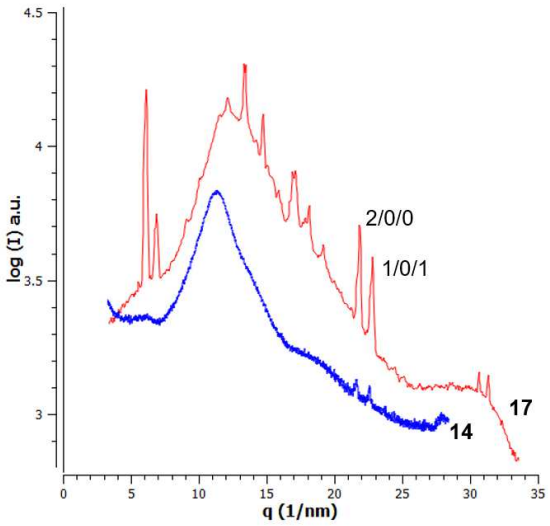

Figure 13: SAXS and WAXS spectrum of Sn@^{micro}1-naphthyl (**17**) (red) compared to Sn@*o*-tolyl (**14**) (blue)

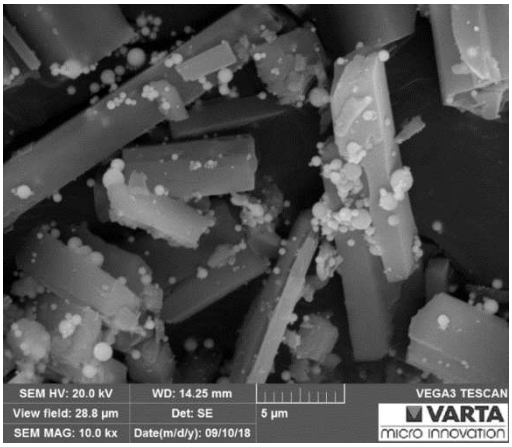

Figure 14: SEM image of Sn@^{micro}1-naph (**17**)

Due to the complication with the 1-naphthyl residue, it was decided to return to the *o*-tolylSnH$_3$ (**6**) as a starting material. It was treated again with 100°C for 20 minutes in DME and the resulting dark brown solution (**18**) showed only the leaving group toluene and the educt **6** (Scheme 15).

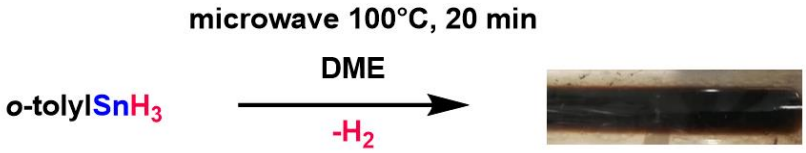

Scheme 15: Microwave assisted synthesis of Sn@^{micro}*o*-tolyl (**18**)

Because the reaction conditions in the first attempt were too mild, a higher temperature of 120°C was applied (Scheme 16). Due to the high temperature, the solvent, as well as the produced hydrogen led to an increase of the pressure during the reaction (Figure 15). The obtained black precipitate Sn@^{micro}*o*-tolyl (**19**) showed again a spherical morphology by investigation with SEM. Further measurements using S(W)AXS display a correlation length of 1.65 nm. Also, GC-MS and EA analysis confirmed the loss of toluene as a leaving group.

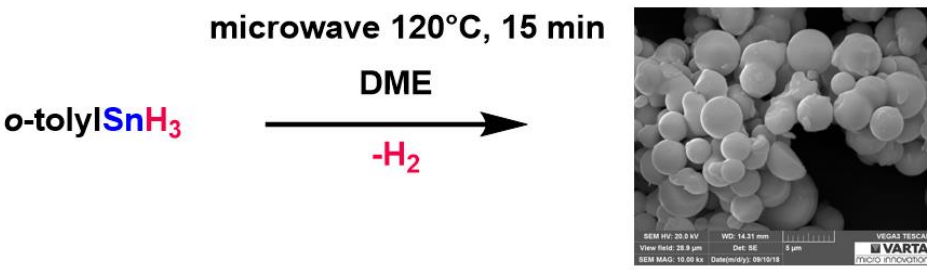

Scheme 16: Microwave assisted synthesis of Sn@^{micro}*o*-tolyl (**19**)

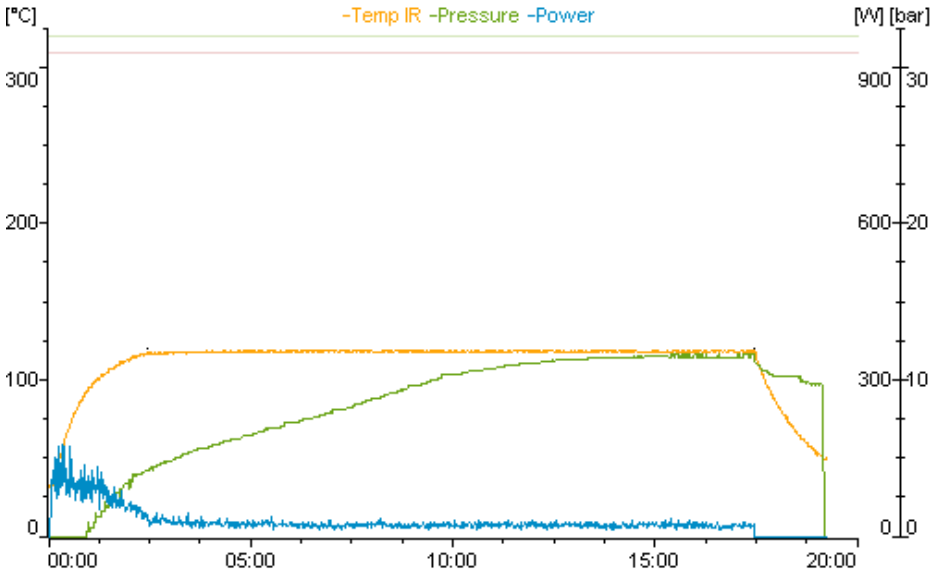

Figure 15: Process diagram of the microwave assisted polymerization towards Sn@^{micro}*o*-tolyl (**19**)

3.5 Intra-amine Catalyzed Dehydrogenation

The working group of Uhlig reported that organotin hydrides easily undergo dehydrogenative coupling reaction upon loss of hydrogen and Sn-Sn bond formation in the presence of amine base TMEDA or thermally induced.[96] Futhermore, monohydrides led to the formation of distannanes, dihydrides produce linear polystannanes and trihydrides result in 3D polymers containing tin and carbon residues. (Sn@aryl).[2]

According to these findings, it is expected that organotin hydrides exhibiting a L^{CN} moiety are unstable too. The already existing amine functionality in the molecule should allow for Sn-H bond cleavage. These compounds should easily form Sn-Sn bonds without addition of an external amine base due to the presence of the intramolecular N→Sn interaction (Figure 16). Moreover, this instability should increase with the number of hydrogens bonded to the tin.

In previous work, it was observed that the formation of organotin monohydrides ($L^{CN}{}_2SnBuH$) (**27**) can be carried out very easily by applying the literature procedure. The hydrogenation of organotin di- and trihalides exhibiting L^{CN} residue applying a similiar method led to undesired dehydrogenative coupling reactions with many side products. This is due to the internal amine functional group leading to a high degree of temperature instability. Therefore, an isolation of the organotin hydrides exhibiting L^{CN} moieties was not possible, as well as a full characterization of the 3D tin-carbon composite materials $Sn@L^{CN}$ (**35**).

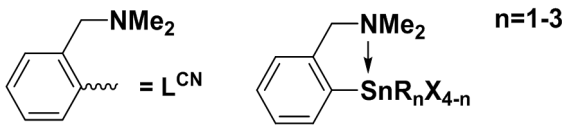

Figure 16: C,N- chelated organotin ligand and N→Sn interaction

3.5.1 Novel Synthesis of C,N-chelated Organotin Polymers

This chapter focuses on the preparation of BX_3 protected C,N-chelated organotin halides as potential precursors for C,N-chelated organotin hydrides, which can be further used to obtain aryl decorated nanoparticles ($Sn@L^{CN}$). The aim of the first reaction is to prepare organotin(IV) species, in which the N→Sn interaction is circumvented by the coordination of the ligand pendant arm to the BX_3 moiety. Next, the protected organotin(IV) halides will be converted to the corresponding hydrides using $K[B(Et)_3H]$ as a hydride source and finally the

protecting group should be removed by adding an amine base or applying temperature in order to form the corresponding distannane, 2D and 3D polymers (Scheme 17).

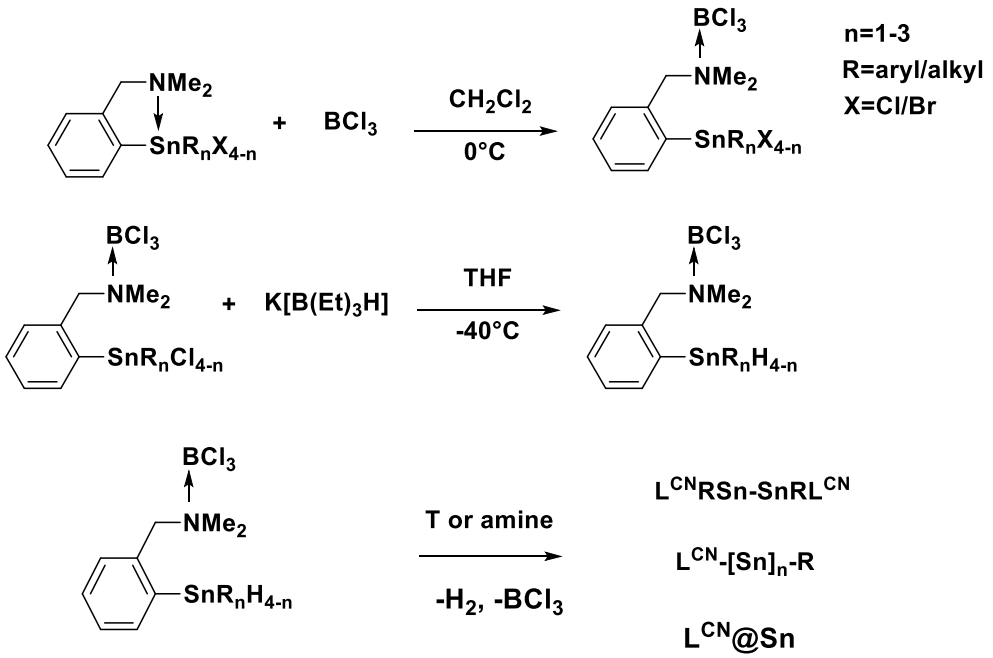

Scheme 17: Preparation of BX_3 protected C,N- chelated organotin halides

3.5.1.1 Synthesis of BX_3 protected C,N- chelated Organotin Halides

The aim of this synthesis was to prepare organotin(IV) species in which the unwanted N→Sn interaction is circumvented by the coordination of the ligand pendant arm to the BX_3 moiety. To the starting C,N-chelated organotin halides (**20, 21, 22, 23, 24, 25, 26**), halogenated BX_3 compounds were added and the reactions were stirred overnight to obtain the desired products (**28, 29, 30, 31, 32, 33, 34**). They were investigated using ^{1}H, ^{11}B, ^{13}C and ^{119}Sn NMR and the obtained data are presented in Tables 1 and 2.

Table 1: ^{119}Sn NMR chemical shift values of prepared compounds measured in $CDCl_3$

compound	^{119}Sn NMR shift (ppm)	compound	^{119}Sn NMR shift (ppm)	$\Delta\delta^{119}$Sn (ppm)	^{11}B NMR shift (ppm)
BCl_3					46.4
BBr_3					38.6
$L^{CN}SnR_2Cl \cdot BCl_3$		**$L^{CN}SnR_2Cl$**			
$L^{CN}SnPh_2Cl \cdot BCl_3$ (**28**)	-48.7	$L^{CN}SnPh_2Cl$ (**20**)	-176.5	127.5	10.0
$L^{CN}SnBu_2Cl \cdot BCl_3$ (**29**)	86.6	$L^{CN}SnBu_2Cl$ (**21**)	-47.5	134.1	10.2
$L^{CN}SnRCl_2 \cdot BCl_3$		**$L^{CN}SnRCl_2$**			
$L^{CN}SnPhCl_2 \cdot BCl_3$ (**30**)	-30.7	$L^{CN}SnPhCl_2$ (**22**)	-167	136.3	10.0
$L^{CN}SnBuCl_2 \cdot BCl_3$ (**31**)	26.4	$L^{CN}SnBuCl_2$ (**23**)	-104.3	130.7	10.2
$L^{CN}SnAr^*Cl_2 \cdot BCl_3$ (**32**)	-27.1	$L^{CN}SnAr^*Cl_2$ (**24**)	-167	139.9	10.0
$L^{CN}SnBr_3 \cdot BBr_3$		**$L^{CN}SnBr_3$**			
$L^{CN}SnBr_3 \cdot BBr_3$ (**34**)	-257.9	$L^{CN}SnBr_3$ (**26**)	-407	149.1	3.2
$L^{CN}{}_2SnBr_2 \cdot BBr_3$		**$L^{CN}{}_2SnBr_2$**			
$L^{CN}{}_2SnBr_2 \cdot BBr_3$ (**33**)	-81.6	$L^{CN}{}_2SnBr_2$ (**25**)	-272	190.4	3.4

^{11}B shifts corresponded nicely to Nöth's results, which declare a NMR shift around 10 ppm for $BCl_3 \cdot NMe_3$ compounds.[107] Furthermore, the $\Delta\delta^{119}Sn$ between the starting materials and $L^{CN}SnR_2Cl \cdot BCl_3$ or $L^{CN}SnRCl_2 \cdot BCl_3$ species was always approximately 130 ppm, which proved the transfer from a five coordinate compound to a four coordinate one.[108] Therefore, the interaction between Sn and N was circumvented by the coordination of the ligand pendant arm to the BX_3 moiety. The ^1H NMR of the starting species $L^{CN}SnR_2Cl$ or $L^{CN}SnRCl_2$, where N→Sn have an interaction, showed always a singlet for the $-N(CH_3)_2$ group in the region of 2.7 ppm. However, the ^1H NMR spectra of the $L^{CN}SnR_2Cl \cdot BCl_3$ or $L^{CN}SnRCl_2 \cdot BCl_3$ species showed a splitting of the proton peak, which also indicated the presence of BX_3 coordinated to the nitrogen. Due to the change of the environment, the protons coupled to the boron and this led to the splitting into a quartet (Figure 17). In Table 2, all the relevant ^1H NMR chemical shift values of prepared compounds measured in $CDCl_3$ are summarized.

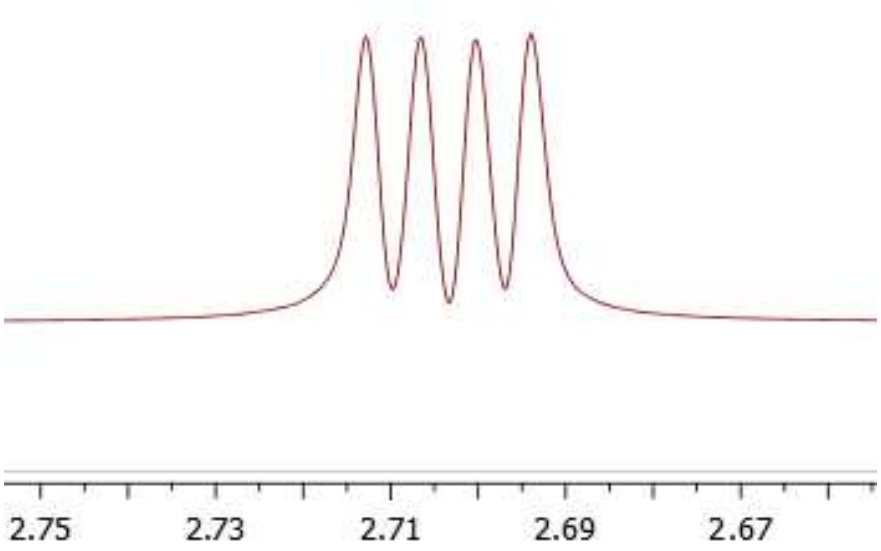

Figure 17: Selected ^1H NMR of the $-N(CH_3)_2$ group of $L^{CN}SnPh_2Cl \cdot BCl_3$ (**28**) measured in $CDCl_3$

Table 2: ^{1}H NMR chemical shift values of prepared compounds measure in $CDCl_3$

compound	-(CH_2)N (ppm)	-N(CH_3)$_2$ (ppm)
$L^{CN}SnR_2Cl \cdot BCl_3$		
$L^{CN}SnPh_2Cl \cdot BCl_3$ (**28**)	4.68	2.71
$L^{CN}SnBu_2Cl \cdot BCl_3$ (**29**)	4.59	2.81
$L^{CN}SnRCl_2 \cdot BCl_3$		
$L^{CN}SnPhCl_2 \cdot BCl_3$ (**30**)	4.62	2.79
$L^{CN}SnBuCl_2 \cdot BCl_3$ (**31**)	4.66	2.89
$L^{CN}SnAr^{*}Cl_2 \cdot BCl_3$ (**32**)	4.67	2.79
$L^{CN}SnBr_3 \cdot BBr_3$		
$L^{CN}SnBr_3 \cdot BBr_3$ (**34**)	4.64	3.08
$L^{CN}{}_2SnBr_2 \cdot BBr_3$		
$L^{CN}{}_2SnBr_2 \cdot BBr_3$ (**33**)	4.71	3.07

The following two compounds, $L^{CN}SnPh_2Cl \cdot BCl_3$ (**28**) and $L^{CN}SnBr_3 \cdot BBr_3$ (**34**), were able to be crystallized out of a mixture of dichloroethane and pentane. Both proved the suggested concept by showing no N→Sn interaction. The distance between Sn and N in these compounds is about 4 Å, in contrast to the non-protected compounds which have a distance about 2 Å (Figure 18).

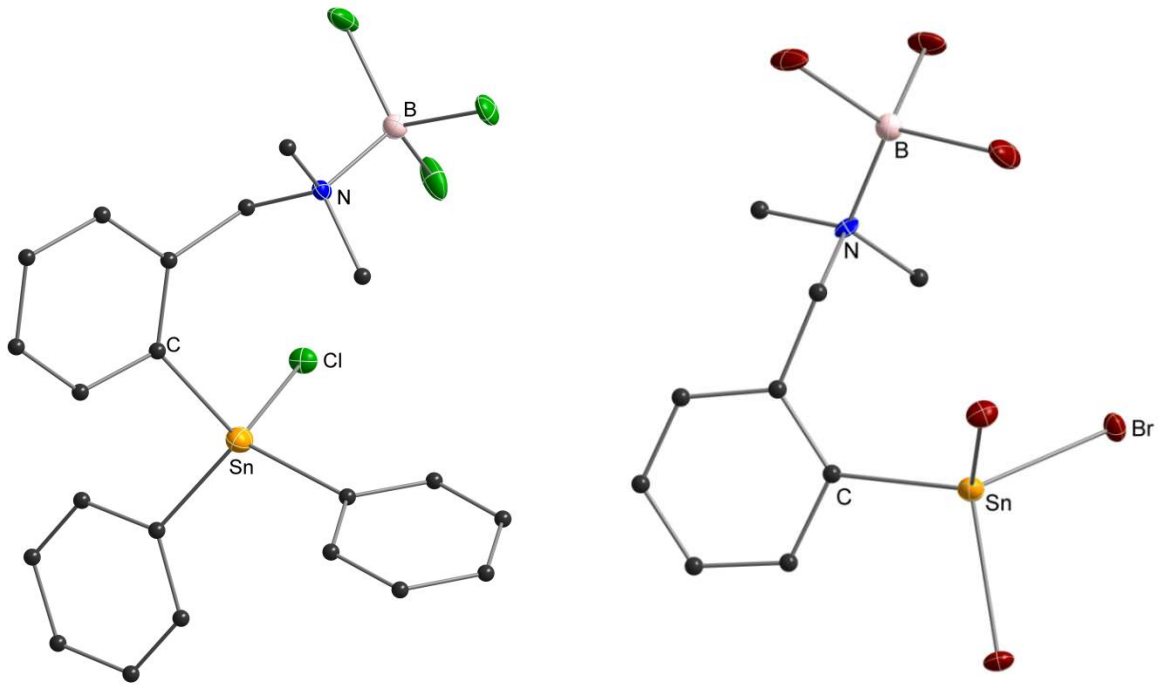

Figure 18: Crystal structures of $L^{CN}SnPh_2Cl \cdot BCl_3$ (**28**) and $L^{CN}SnBr_3 \cdot BBr_3$ (**34**)

3.5.1.2 Proposed Mechanism Towards the Side Product

Due to excess of BX_3 in order to obtain the protected C,N-chelated organotin halides, a stable side product $[(L^{CN})_2SnCl_3]^+ \cdot ½\ [SnCl_6]^{2-}$ (**36**) was formed (Scheme 18). This compound was generated by the proposed mechanism below and it is suggested that this could be the limiting factor of the reaction towards the $L^{CN}SnRH_2 \cdot BCl_3$. The side product was obtained as a crystalline solid with a melting point of 210-212°C and due to the fact that it was not soluble in any solvent, no NMR spectrum could be recorded (Figure 19).

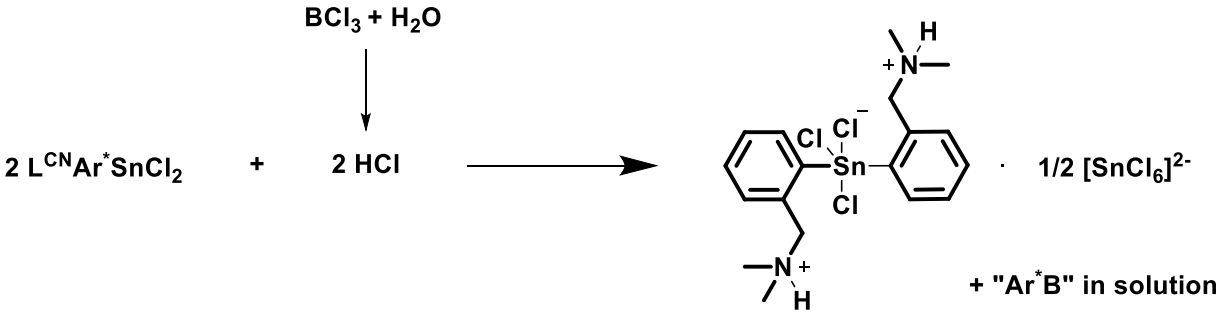

Scheme 18: Proposed reaction mechanism for the stable side product **36**

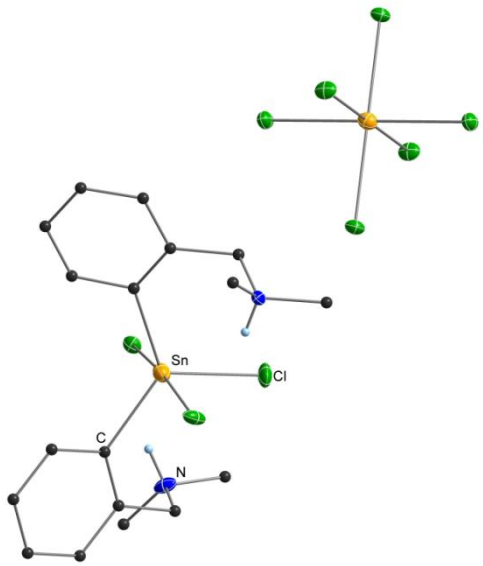

Figure 19: Crystal structure of $[(L^{CN})_2SnCl_3]^+ \cdot ½\ [SnCl_6]^{2-}$ (**36**)

3.5.1.3 Synthesis of $L^{CN}SnBu_2H \cdot BCl_3$

Before starting the hydrogenation of $L^{CN}SnBu_2Cl \cdot BCl_3$ (**29**), the stability of the monochloride in THF was examined by measuring the starting material in d^8-THF. The ^{119}Sn NMR value shifted from +86.6 ppm to +26.6 ppm, which can be explained by the fact that THF is a coordinating solvent which interacts which the Sn center. The interaction between THF and Sn, results in loosening of the Sn-Cl bond which is a perfect condition for the hydrogenation.

The hydrogenation towards $L^{CN}SnBu_2H \cdot BCl_3$ (**29**) was carried out by using $K[B(Et)_3H]$. After few minutes stirring, the reaction was finished, and the desired product could be isolated by filtration. However, the presence of the butyl residue hindered the isolation of crystalline materials. In the ^{119}Sn spectrum, the desired product **29** was found at -118.4 ppm and showed expected splitting when measured in ^1H coupling mode. The $^1J(^{119}Sn\text{-}^1H)$ and $^1J(^{117}Sn\text{-}^1H)$ values (1720 and 1644 Hz) agree very well with the reported coupling constants concerning tin hydrides (Figure 20).[1]

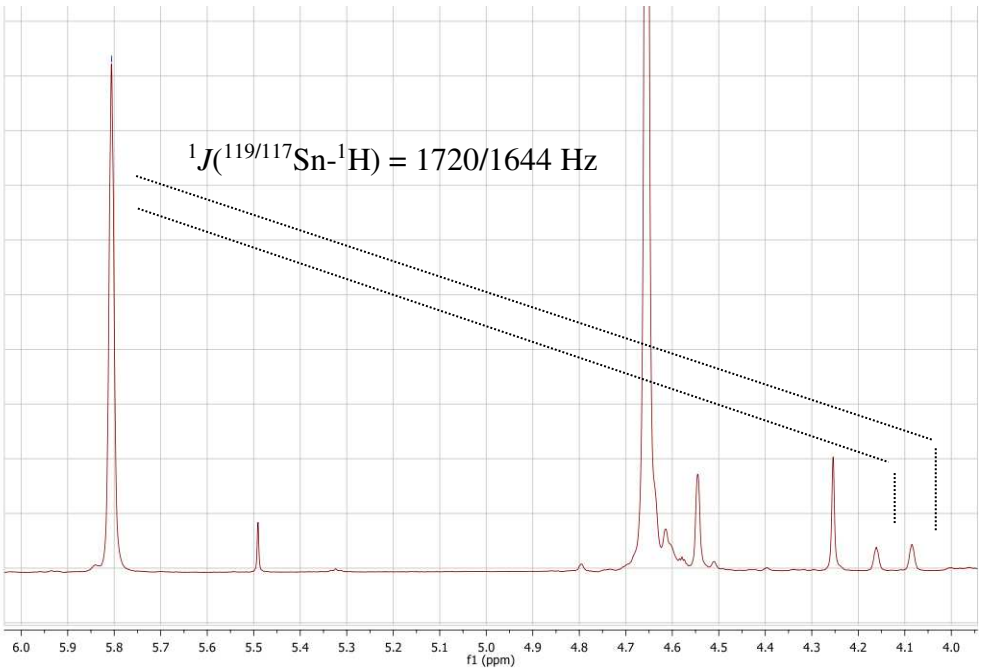

Figure 20: Selected regions of the ^1H spectrum of $L^{CN}SnBu_2H \cdot BCl_3$ (**29**) in d^8-THF. $^1H\text{-}^{119/117}Sn$ coupling patterns are indicated by dotted lines.

3.5.1.4 Stability of $L^{CN}SnBu_2H \cdot BCl_3$ Against Amine Bases

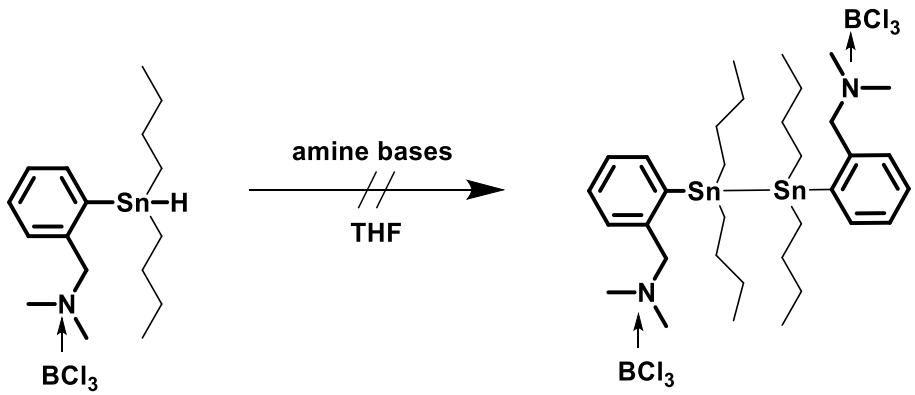

Scheme 19: Attempted of synthesizing a distannane adding different amine bases

Uhlig *et al.* reported that organotin hydrides easily undergo dehydrogenative coupling reactions upon loss of hydrogen and Sn-Sn bond formation in the presence of amine base TMEDA.[96] Hence, monohydrides led to a quantitative formation of distannanes, dihydrides generate linear polystannanes and trihydrides result in nonporous tin-carbon composite materials ($Sn@L^{CN}$).[1] In order to obtain the distannane of the starting $L^{CN}SnBu_2H \cdot BCl_3$ (**29**), it was treated with different amine bases. Unfortunately, the hydride showed no reaction with either of these reaction agents. Due to the fact, that the Sn-H bond is quite strong, the presence of an amine base was not capable of cleaving the hydrogen (Scheme 19).

3.5.1.5 Conversion of $L^{CN}SnBr_3 \cdot BBr_3$ *via* the Corresponding Hydrides Towards $Sn@L^{CN}$

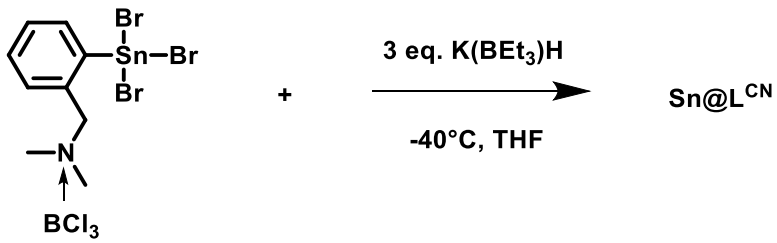

Scheme 20: Synthesis of aryl decorated tin nanoparticles $Sn@L^{CN}$ (**35**)

Due to the reason that the trihydride is the most reactive hydride, the hydrogenation of the starting $L^{CN}SnBr_3 \cdot BBr_3$ (**34**) went directly towards the aryl decorated tin nanoparticles **35** (Scheme 20). However, due to the presence of the BX_3 protecting group, weakening the intramolecular interaction of the pendant amine arm with the tin, the polymerization reaction was slowed down during the polymerization procedure, but the direct polymerization could not be avoided. The resulting product was examined by EA, SEM, SAXS and WAXS.

Elemental Analysis showed a carbon content of 4.90% and a hydrogen content around 0.79% which indicated a high amount of Sn in the obtained polymer **35**. But the following SEM and EDX measurements showed that the aryl decorated tin nanoparticles **35** were completely covered in KBr salt, which was a side product of the hydrogenation reaction (Figure 21).

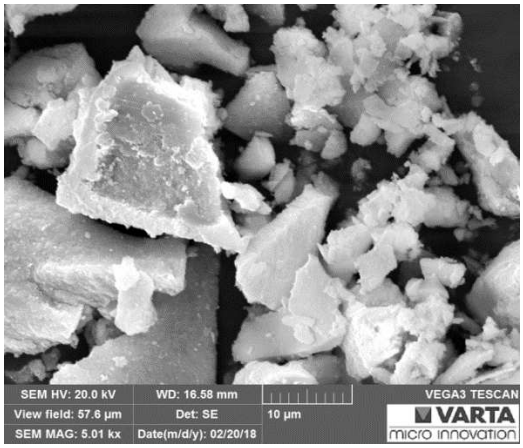

Figure 21: SEM measurement of the obtained polymer **35**

Furthermore, SAXS displayed a peak at low angle related to large particles and WAXS reflexes that corresponding to KBr peaks from XRD also confirm, as seen in the SEM, the presence of the salt (Figure 22). In order to get rid of the covering salt layer, the polymer was washed with water and measured again. Unfortunately, the KBr could not be removed.

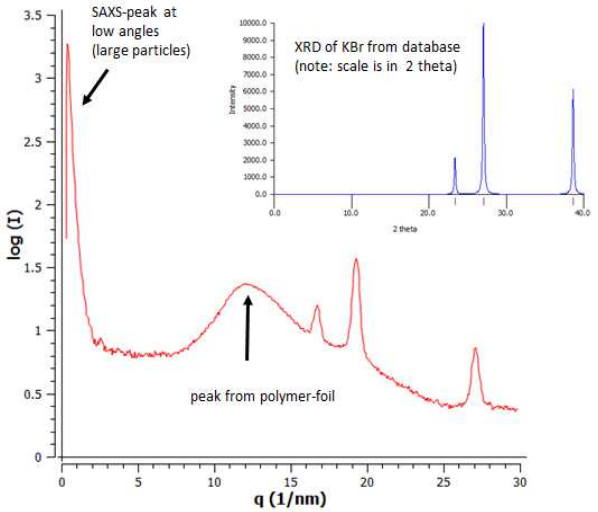

Figure 22: SAXS and WAXS measurement of the obtained polymer

4 Summary & Outlook

In the course of this master thesis a series of different methods influencing the dehydrogenative coupling reaction of arylSnH$_3$ with different ligand systems was investigated. In summary, a model system involving fast and slow polymerization methods can be suggested. Applying a strong amine base to the hydride or using microwave assisted polymerization led to the formation of spherical aryl decorated nanoparticles, which differ in their size, but not in their shape. Using further treatment with ultrasonication within the amine induced dehydrogenative coupling, the morphology starts to change towards more stacked-together particles. Furthermore, due to the fact that all of the morphologies obtained by fast polymerization methods have a very organized macrostructure, correlation lengths could be measured (Figure 23).

In contrast to the polymers produced by an amine base or microwave, the thermally induced dehydrogenative coupling without an amine base resulted in a much slower polymerization method. SEM images showed that the macrostructure no longer consists of these spherical particles, but display plates, which are stacked together. Moreover, the same phenomena concerning the sonication experiment can be observed here too. Due to the longer reaction time, the aryl decorated nanoparticles have more time to organize themselves and can lose more of the remaining hydrogen and organic residue in the tin core. Therefore, WAXS measurements display distinct reflections which can be assigned to white tin (Figure 23).

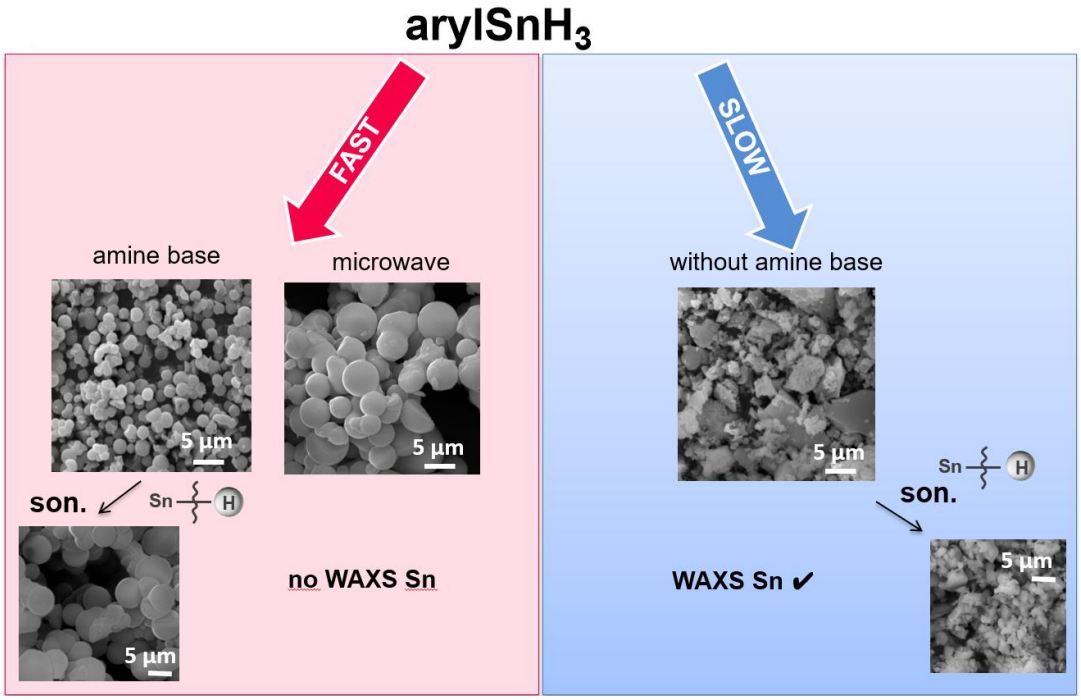

Figure 23: Suggested model concerning fast and slow polymerization methods

In addition, a variety of BX_3 protected C,N-chelated organotin halides were able to be isolated and characterized by ^{1}H, ^{11}B, ^{13}C and ^{119}Sn NMR. Two crystal structures, $L^{CN}SnPh_2Cl \cdot BCl_3$ (**28**) and $L^{CN}SnBr_3 \cdot BBr_3$ (**34**), could also be successfully obtained. The conversion towards the corresponding hydrides did not proceed, due to the formation of a side product in the first reaction step. However, the monohydride $L^{CN}SnBu_2H \cdot BCl_3$ was synthesized and characterized by NMR studies. Stability tests of this compound against a carbene, as well as amine bases were carried out. Finally, the attempt to hydrogenate $L^{CN}SnBr_3 \cdot BBr_3$ resulted in the direct formation of aryl decorated nanoparticles which were completely covered in potassium bromide. Unfortunately, the salt layer could not be removed by washing.

Novel electrode materials is one of the most active research areas in material science since lithium ion batteries (LIBs) are considered as the choice for energy storage.[109, 110] The standard graphite anodes have a very low theoretical capacity of 372 mAh/g and therefore alternatives are searched. Recently, incooperation of tin into these systems is one of the key research topics due to the high theoretical capacity of tin of 944 mAh/g, its high abundance and low price. The big drawback of tin materials is the enormous volume change of about 300% when being charged.[111-113] This problem can be improved by using tin based materials at the nanoscale, due to the increasing number of active sites and a higher ability to buffer the volume expansion.[109, 110, 112, 114, 115]

The working group of Uhlig recently investigated the formation of nanostructured composites of tin and carbon-based nanoparticles. These can either be produced by mixing the graphite layer with the aryl decorated tin nanoparticles or by an *in situ* dehydrogenative polymerization using the amine base TMEDA in the presence of a graphite surface (Figure 24). In both methods, CV (Capacitance-Voltage) measurements provided promising results.[116] Therefore, the next step is to test all synthesized materials against their electrochemical performance, including rate capability, specific capacity, and cycling stability.

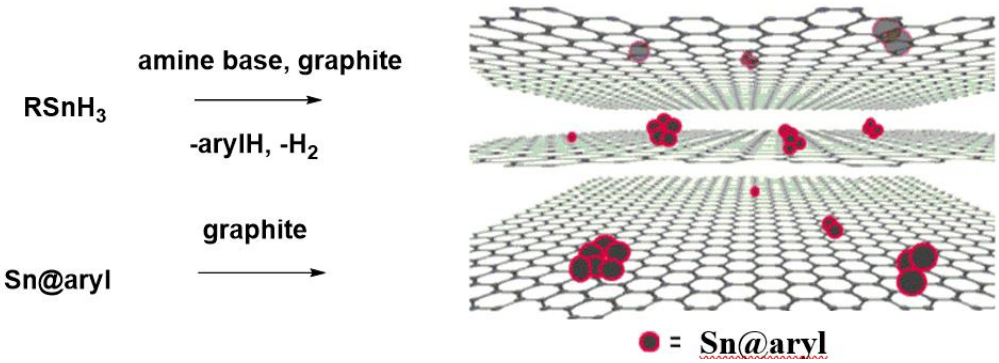

Figure 24: Formation of nanostructured composites of tin and carbon-based nanoparticles

5 Experimental Part

5.1 Materials and Methods

The following reactions were carried out using Schlenk line techniques under argon or nitrogen atmosphere. Solvents were obtained from a solvent drying system (Innovative Technology, Inc.), $SnCl_4$ (**1**) anhydrous (98 % v/v), C_6D_6 (deuterated benzene) and TMEDA (*N*,*N*,*N'*,*N'*-tetramethylethylenediamine) were distilled and stored under inert gas. All other chemicals were utilized without further purification.

5.2 NMR Spectroscopy

^{1}H (300.22 MHz), ^{13}C (75.5 MHz)), ^{11}B (96 MHz) and ^{119}Sn (111.92 MHz) NMR spectra were recorded on a Mercury 300 MHz spectrometer from Varian at 25°C if not otherwise stated. Chemical shifts are given in parts per million (ppm) relative to TMS (δ= 0 ppm) regarding ^{13}C and ^{1}H and relative to Me_4Sn in the case of ^{119}Sn. Coupling constants (*J*) are reported in Hertz (Hz). The letters s, d, t, q and m are used to indicate singlet, doublet, triplet, quadruplet and multiplet.

5.3 GC-MS Measurements

GC-MS measurements were carried out on an Agilent Technologies 7890A GC system coupled with an Agilent Technologies 5975C VLMSD mass spectrometer using a HP5 column (30 m×0.250mm×0.025 µm) and a carrier helium gas flow of 0.92726 ml/min. A „hot-needle“, manual injection method at an injector temperature of 280°C was performed. After 2 min at 40°C the temperature was increased in 12°C/min steps up to 300°C and kept at 300°C for 10 min. The MS conditions included positive EI ionization at an ionization energy of 70 eV and a full scan mode (50-500 m/z).

5.4 Crystal Structure Determination

The X-ray data (Table 3) for colorless crystals of all compounds were obtained at 150 K using Oxford Cryostream low-temperature device on a Nonius KappaCCD diffractometer with MoK_α radiation (λ = 0.71073 Å), a graphite monochromator, and the φ and χ scan mode. Data reductions were performed with DENZO-SMN.[117] The absorption was corrected by integration methods. Structures were solved by direct methods (Sir92)[118] and refined by full matrix least-square based on F^2 (SHELXL97).[119] Hydrogen atoms were mostly localized on a difference Fourier map, however to ensure uniformity of the treatment of the crystal, all hydrogen atoms were recalculated into idealized positions (riding model) and assigned temperature factors $H_{iso}(H)=1.2\ U_{eq}$ (pivot atom) or of $1.5U_{eq}$ for the methyl moiety with C–H = 0.96, 0.97, and 0.93 Å for methyl, methylene and hydrogen atoms in aromatic rings, respectively, and 0.82 Å for N–H and O–H groups.

5.5 Powder Diffraction Studies

The sample was transferred into a quartz glass capillary (OD: 1.5 nm) in the glove box and flame sealed. X-Ray powder diffraction (XRPD) patterns were recorded on a Bruker D8 Advance diffractometer with Bragg Brentano geometry using Cu Kα radiation (9–100° 2ϑ, step size 0.02° 2ϑ, step time 30s/step) and a LYNXEYE detector. Rietveld refinement was carried out with X-PertHighScorePlus (PANalytical) and Topas (Bruker).

5.6 Elemental Analysis

Elemental analysis was performed with an Elementar Vario EL III.

5.7 SAXS and WAXS Measurements

Solid powder samples were transferred in the glove box into a sealable (by screw caps) sample holder (Anton Paar, Graz, Austria) where the sample was sandwiched (1 mm) between two vacuum-tight sealing polycarbonate foils (100 µm each). Small-angle (wide-angle) X-ray scattering, S(W)AXS, measurements were carried by a high-flux SAXSess camera (Anton Paar, Graz, Austria) connected to a Debye flex 3003 X-ray generator (GE-Electric, Germany), operating at 40 kV and 50 mA with a sealed-tube Cu anode. The Goebel mirror focused and Kratky slit collimated X-ray beam was line shaped (17 mm horizontal dimension at the sample) and scattered radiation from the sample in the SAXS-range was recorded by a one-dimensional MYTHEN-1k microstrip solid-state detector (Dectris, Switzerland) for 200 s

within a q-range of 0.1 to 5 nm^{-1} (with q being the magnitude of the scattering vector). Additionally, also WAXS data were recorded separately by a highly X-ray sensitive image plates (Fuji, Japan) within a q-range up to 25 nm^{-1}. After each SWAXS measurement with an exposure time of 5 min, the image plates were transferred to a Cyclone Plus image plate reader (Perkin Elmer, USA), laser-scanned and converted digitally into intensity values (I). The 2D recorded intensity data were then integrated with a 10 mm width, normal to the direction of the scattering angle, to result in a 1D-scattering curve $I(q)$ within the angular range mentioned above. Converting the q-scale into 2θ (°), with 2θ being the scattering angle with respect to the incident beam and λ the wavelength of the X-rays, the maximal q-value would correspond to an angular rage of 7° (SAXS) and 40° (SWAXS), using CuKα radiation of wavelength 0.154 nm and a sample-to-detector distance of 309 mm (SAXS) and 269 mm (SWAXS), respectively.

5.8 SEM Measurements

Scanning electron microscopy (SEM) analysis was performed on a Vega 3 SBU SEM with a tungsten hair-pin cathode. Non-conductive samples were sputtered with gold for topographic characterization. Qualitative and quantitative analysis of the layers and particles was performed *via* energy dispersive X–ray microanalysis (EDX) (Oxford Instruments, model INCA X-act).

5.9 Microwave

The sample was transferred into a 10 mL microwave vial and the reaction was performed in the Microwave Synthesis Reactor Monowave 300 from Anton Paar.

5.10 Sonication Bath

The sonication experiments were performed with Elmasonic S 30 and a cooling coil. The bath has an ultrasonic frequency of 37 kHz and a power effect of 80 W. The maximal filling volume of the tank is 2.75 L.

5.11 Synthesis

List of Compounds

	Compound	no.
	$SnCl_4$	**1**
Ar_4Sn	*o*-tolyl$_4$Sn	**2**
	1-naphthyl$_4$Sn	**3**
$ArSnCl_3$	*o*-tolyl$SnCl_3$	**4**
	1-naphthyl$SnCl_3$	**5**
$ArSnH_3$	*o*-tolylSnH_3	**6**
	2,4,6-mesSnH_3	**7**
	1-naphthylSnH_3	**8**
	$PhSnH_3$	**9**
H_2[(aryl)Sn–Sn(aryl)]H_2	H_2[(*o*-tolyl)Sn–Sn(*o*-tolyl)]H_2	**10**
	H_2[(phenyl)Sn–Sn(phenyl)]H_2	**11**
Ar@Sn	Sn@$^{1\text{ eq. TMEDA}}$*o*-tolyl (RT, 20 min)	**12**
	Sn@$^{0.1\text{ eq. TMEDA}}$*o*-tolyl (RT, 45 min)	**13**
	Sn@*o*-tolyl (RT, 16 days)	**14**
	Sn@^{son}*o*-tolyl (RT, 20 days)	**15**
	Sn@$^{son,\text{ 1 eq. TMEDA}}$*o*-tolyl (RT, 30 min)	**16**
	Sn@^{micro}1-naphthyl (100°C, 20 min)	**17**
	Sn@^{micro}*o*-tolyl (100°C, 20 min)	**18**
	Sn@^{micro}*o*-tolyl (120°C, 15 min)	**19**
L^{CN}Sn halogenides	$L^{CN}SnPh_2Cl$	**20**
	$L^{CN}SnBu_2Cl$	**21**
	$L^{CN}SnPhCl_2$	**22**
	$L^{CN}SnBuCl_2$	**23**
	$L^{CN}SnAr^*Cl_2$	**24**
	$L^{CN}{}_2SnBr_2$	**25**
	$L^{CN}SnBr_3$	**26**
L^{CN}Sn hydride	$L^{CN}{}_2SnBuH \cdot BCl_3$	**27**
L^{CN}Sn halogenides · BCl_3	$L^{CN}SnPh_2Cl \cdot BCl_3$	**28**
	$L^{CN}SnBu_2Cl \cdot BCl_3$	**29**
	$L^{CN}SnPhCl_2 \cdot BCl_3$	**30**
	$L^{CN}SnBuCl_2 \cdot BCl_3$	**31**
	$L^{CN}SnAr^*Cl_2 \cdot BCl_3$	**32**
	$L^{CN}{}_2SnBr_2 \cdot BBr_3$	**33**
	$L^{CN}SnBr_3 \cdot BBr_3$	**34**
L^{CN}Sn polymer	Sn@L^{CN}	**35**
L^{CN} side product	$[(L^{CN})_2SnCl_3]^+ \cdot ½\ [SnCl_6]^{2-}$	**36**

5.11.1 Published Compounds

The following compounds were synthesized according to literature known procedures and only the ^{1}H, ^{119}Sn, ^{13}C and ^{11}B NMR data is provided.

$SnCl_4$ 1: ^{119}Sn NMR (C_6D_6, 112 MHz): δ -148.6 ppm.

***o*-tolyl$_4$Sn 2:** ^{1}H NMR ($CDCl_3$, 300 MHz): δ = 7.53 (d, 4H, ^{3}J(H-H) = 7.6 Hz, ^{3}J(^{117}Sn-H) = 39.2 Hz, ^{3}J(^{119}Sn-H) = 53.8 Hz ppm), 7.31-7.23 (m, 8H), 7.19-7.11 (m, 4H). ^{119}Sn NMR ($CDCl_3$, 112 MHz): δ = –121.8 ppm.

1-naphthyl$_4$Sn 3: ^{1}H NMR (C_6D_6, 300 MHz): δ 8.33 (d, 4H, ^{3}J(H4-H3) = 8.3 Hz, H4), 8.12 (d, 4H, ^{3}J(H2-H3) = 6.6 Hz, H2), 7.62 (d, 4H, ^{3}J(H8-H7) = 8.2 Hz, H8), 7.54 (d, 4H, ^{3}J(H5-H6) = 8.1 Hz, H5), 7.12-7.00 (m, 8H, H6, H7), 6.83 (dd, 2H, H3) ppm. ^{13}C NMR (C_6D_6, 75.5 MHz): δ 140.7 (^{1}J(^{13}C-^{119}Sn) = 520 Hz, ^{1}J(^{13}C-^{117}Sn) = 497 Hz, C1), 139.4 (^{2}J(^{13}C-^{119}Sn) = 34.7 Hz, ^{2}J(^{13}C-^{117}Sn) = 33.8 Hz, C8a), 137.6 (^{2}J(^{13}C-$^{119/117}$Sn) = 38.1 Hz, C2), 134.5 (^{3}J(^{13}C-^{119}Sn) = 37.6 Hz, ^{3}J(^{13}C-^{117}Sn) = 36.4 Hz, C4a), 130.6 (^{4}J(^{13}C-$^{119/117}$Sn) = 32.2 Hz, C4), 130.3 (^{3}J(^{13}C-$^{119/117}$Sn) = 11.7 Hz, C8), 129.3 (^{3}J(^{13}C-$^{119/117}$Sn) = 43.8 Hz, C3), 126.4 (C7), 126.1 (C6) ppm. ^{119}Sn NMR (C_6D_6, 112 MHz): δ -118.8 ppm.

***o*-tolylSnCl_3 4:** ^{1}H NMR (C_6D_6, 300 MHz): δ 7.21 (d, 1H, ^{3}J(H6-H5) = 8.5 Hz, ^{4}J (H6-$^{119/117}$Sn) = 64.6 Hz, H6), 7.06-6.97 (dd, 1H, H4), 6.91-6.82 (dd, 1H, H5), 6.81-6.76 (d, 1H, H3), 2.18 (s, 3H, ^{4}J(H7-$^{119/117}$Sn) = 13.7 Hz, H6) ppm. ^{13}C NMR (C_6D_6, 75.5 MHz): δ 142.9 (^{2}J(^{13}C-^{119}Sn) = 75.2 Hz, ^{2}J(^{13}C-^{117}Sn) = 72.0 Hz, C2), 136.7 (^{1}J(^{13}C-^{119}Sn) = 1085 Hz, ^{1}J(^{13}C-^{117}Sn) = 1036 Hz, C1), 134.4 (^{2}J(^{13}C-^{119}Sn) = 77.8 Hz, ^{2}J(^{13}C-^{117}Sn) = 74.4 Hz, C6), 133.3 (^{4}J(^{13}C-$^{119/117}$Sn) = 23.9 Hz, C4), 131.6 (^{3}J(^{13}C-^{119}Sn) = 119 Hz, ^{3}J(^{13}C-^{117}Sn) = 114 Hz, C3), 127.2 (^{3}J(^{13}C-^{119}Sn) = 128 Hz, ^{3}J(^{13}C-^{117}Sn) = 122 Hz, C5), 24.3 (^{3}J(^{13}C-^{119}Sn) = 55.3 Hz, ^{3}J(^{13}C-^{117}Sn) = 53.4 Hz, C7) ppm. ^{119}Sn NMR (C_6D_6, 112 MHz): δ -60.7 ppm.

1-naphthylSnCl_3 5: ^{1}H NMR (C_6D_6, 300 MHz): δ 7.97-7.89 (dd, 1H, H6), 7.50-7.30 (m, 3H, H2, H4, H5), 7.12-7.03 (m, 2H, H7, H8), 6.91-6.83 (m, 1H, H3) ppm. ^{13}C NMR (C_6D_6, 75.5 MHz): δ 136.1 (^{1}J(^{13}C-^{119}Sn = 1098 Hz, ^{1}J(^{13}C-^{117}Sn = 1050 Hz, C1), 135.1 (^{2}J(^{13}C-^{119}Sn = 85.5 Hz, ^{2}J(^{13}C-^{117}Sn = 81.7 Hz, C8a), 134.8 (^{3}J(^{13}C-^{119}Sn = 103 Hz, ^{3}J(^{13}C-^{117}Sn = 98.3 Hz, C4a), 134.7 (^{2}J(^{13}C-$^{119/117}$Sn = 63.4 Hz, C2), 133.3 (^{4}J(^{13}C-$^{119/117}$Sn = 27.5 Hz, C4), 129.4 (^{4}J(^{13}C-$^{119/117}$Sn = 20.7 Hz, C5), 128.7 (^{4}J(^{13}C-$^{119/117}$Sn = 6.9 Hz, C7), 125.5 (^{3}J(^{13}C-$^{119/117}$Sn

= 58.3 Hz, C8), 127.3 (C6), 125.8 ($^{3}J(^{13}C\text{-}^{119}Sn$ = 141 Hz, $^{3}J(^{13}C\text{-}^{117}Sn$ = 135 Hz, C3) ppm. ^{119}Sn NMR (C_6D_6, 112 MHz): δ -62.3 ppm.

***o*-tolylSnH$_3$ 6:** ^{1}H NMR (C_6D_6, 300 MHz): δ 7.47 (d, 1H, ^{3}J(H6-H5) = 8.4 Hz, ^{4}J (H6-$^{119/117}Sn$) = 70.5 Hz, H6), 7.26-7.16 (dd, 1H, H5), 7.14-7.03 (m, 2H, H4, H3), 4.96 (s, 3H, $^{1}J(^{1}H\text{-}^{119}Sn)$ = 1908 Hz, $^{1}J(^{1}H\text{-}^{117}Sn)$ = 1823 Hz, SnH_3), 2.15 (s, 3H, $^{4}J(^{1}H\text{-}^{119/117}Sn)$ = 5.3, H7) ppm. ^{13}C NMR (C_6D_6, 75.5 MHz): δ 144.8 ($^{2}J(^{13}C\text{-}^{119}Sn)$ = 33.4 Hz, $^{2}J(^{13}C\text{-}^{117}Sn)$ = 31.7 Hz, C2), 139.0 ($^{2}J(^{13}C\text{-}^{119}Sn)$ = 45.0 Hz, $^{2}J(^{13}C\text{-}^{117}Sn)$ = 43.5 Hz, C6), 134.4 ($^{1}J(^{13}C\text{-}^{119}Sn)$ = 568 Hz, $^{1}J(^{13}C\text{-}^{117}Sn)$ = 542 Hz, C1), 129.8 ($^{4}J(^{13}C\text{-}^{119/117}Sn)$ = 11.6 Hz, C4), 129.4 ($^{3}J(^{13}C\text{-}^{119}Sn)$ = 43.5 Hz, $^{3}J(^{13}C\text{-}^{117}Sn)$ = 42.2 Hz, C3), 126.0 ($^{3}J(^{13}C\text{-}^{119}Sn)$ = 58.6 Hz, $^{3}J(^{13}C\text{-}^{117}Sn)$ = 56.2 Hz, C5), 25.8 ($^{3}J(^{13}C\text{-}^{119}Sn)$ = 40.9 Hz, $^{3}J(^{13}C\text{-}^{117}Sn)$ = 39.7 Hz, C7) ppm. ^{119}Sn NMR (C_6D_6, 112 MHz): δ -358.4 ($^{1}J(^{119}Sn\text{-}^{1}H)$ = 1920 Hz) ppm.

1-naphthylSnH$_3$ 8: ^{1}H NMR (C_6D_6, 300 MHz): δ 7.70-7.63 (m, 1H, H8), 7.62-7.53 (m, 2H, H4, H5), 7.48 (d, 1H, ^{3}J(H2-H3) = 6.5 Hz, ^{3}J(H2-$^{119/117}Sn$ = 14.8 Hz, H2), 7.28-7.18 (m, 2H, H6, H7), 7.16-7.09 (dd, 1H, H3), 5.14 (s, 3H, $^{1}J(^{1}H\text{-}^{119}Sn)$ = 1934 Hz, $^{1}J(^{1}H\text{-}^{117}Sn)$ = 1848 Hz, SnH_3) ppm. ^{13}C NMR (C_6D_6, 75.5 MHz): δ 139.1 ($^{2}J(^{13}C\text{-}^{119/117}Sn$ = 35.8 Hz, C8a), 138.2 ($^{2}J(^{13}C\text{-}^{119/117}Sn$ = 39.2 Hz, C2), 134.4 ($^{1}J(^{13}C\text{-}^{119}Sn$ = 534 Hz, $^{1}J(^{13}C\text{-}^{117}Sn$ = 510 Hz, C1), 134.1 ($^{3}J(^{13}C\text{-}^{119/117}Sn$ = 37.6 Hz, C4a), 130.7 ($^{3}J(^{13}C\text{-}^{119/117}Sn$ = 42.4 Hz, C8), 130.0 ($^{4}J(^{13}C\text{-}^{119/117}Sn$ = 12.6 Hz, C4), 129.2 ($^{4}J(^{13}C\text{-}^{119/117}Sn$ = 7.16 Hz, C5), 126.6 (C6), 126.0 ($^{4}J(^{13}C\text{-}^{119/117}Sn$ = 10.9 Hz, C7), 125.9 ($^{3}J(^{13}C\text{-}^{119}Sn$ = 64.5 Hz, $^{3}J(^{13}C\text{-}^{117}Sn$ = 61.6 Hz, C3) ppm. ^{119}Sn NMR (C_6D_6, 112 MHz): δ -353.9 ($^{1}J(^{119}Sn\text{-}^{1}H)$ = 1953 Hz) ppm.

H$_2$[(*o*-tolyl)Sn-Sn(*o*-tolyl)]H$_2$ 10: ^{1}H NMR (C_6D_6, 300 MHz): δ 7.47 (d, 2H, $^{3}J(^{1}H\text{-}^{119/117}Sn)$ = 62.6 Hz, H6), 7.13-6.85 (m, 6H, H3-H5), 5.07 (s, 4H, $^{1}J(^{1}H\text{-}^{119}Sn)$ = 1734 Hz, $^{1}J(^{1}H\text{-}^{117}Sn)$ = 1656 Hz, $^{2}J(^{1}H\text{-}^{119/117}Sn)$ = 135 Hz, $^{3}J(^{1}H\text{-}^{1}H)$ = 3.9 Hz, Sn-H), 2.19 (s, 6H, CH_3) ppm. ^{13}C NMR (C_6D_6, 75.5 MHz): δ 144.8 (C2), 139.2 ($^{4}J(^{13}C\text{-}^{119/117}Sn)$ = 12.3 Hz, C4), 135.5 (C1), 129.8 (C6), 129.5 (C5), 126.1 ($^{3}J(^{13}C\text{-}^{119/117}Sn)$ = 56.0 Hz, C3), 26.1 (C7) ppm. ^{119}Sn (^{1}H coupled) NMR (C_6D_6, 112 MHz): -370.7 (tt, $^{1}J(^{119}Sn\text{-}^{1}H)$ = 1734 Hz, $^{2}J(^{1}H\text{-}^{119}Sn)$ = 135 Hz) ppm.

L^{CN}SnPh$_2$Cl 20: ^{1}H NMR ($CDCl_3$, 300 MHz): δ 8.53 (d, 1H, H(6)); 7.73 (d, 4H, *o*-Ph); 7.46-7.42 (m, 8H, L^{CN} and Ph moieties); 7.22 (m, 1H, H(3)); 3.56 (s, 2H, CH_2N); 1.89 (m, 6H, NMe_2) ppm. ^{119}Sn NMR ($CDCl_3$, 112 MHz): δ -117.1 ppm

$L^{CN}SnBu_2Cl$ 21: ^{1}H NMR ($CDCl_3$, 300 MHz): δ 8.21 (d, 1H, H(6)); 7.25-7.13 (m, 3H, H(3, 4, 5)); 3.56 (s, 2H, CH_2N); 2.27 (m, 6H, NMe_2); 1.70 (br m, 4H, α-CH_2); 1.36 (br, 4H, β-CH_2); 1.36 (sext, 4H, γ-CH_2); 0.88 (t, 6H, δ-CH_3) ppm. ^{119}Sn NMR ($CDCl_3$, 112 MHz): δ -51.7 ppm

$L^{CN}SnPhCl_2$ 22: ^{1}H NMR ($CDCl_3$, 500 MHz): δ 8.33 (d, 1H, H(6), $^{3}J(^{119}Sn, ^{1}H)$ = 100 Hz); 7.67-7.44 (m, 5H, Ph moieties), 7.46 (m, 2H, H(4,5)); 7.25 (d, 1H, H(3)); 3.71 (s, 2H, CH_2N); 2.19 (m, 6H, NMe_2) ppm. ^{119}Sn NMR ($CDCl_3$, 112 MHz): δ -170 ppm.

$L^{CN}SnBuCl_2$ 23: ^{1}H NMR ($CDCl_3$, 300 MHz): δ 8.14 (d, 1H, H(6)); 7.45-7.18(m, 3H, H(3,4, 5)); 3.71 (s, 2H, CH_2N); 2.39 (m, 6H, NMe_2); 1.89 (br m, 4H, α-CH_2); 1.79 (br, 4H, β-CH_2); 1.44 (m, 4H, γ-CH_2); 0.93 (t, 6H, δ-CH_3) ppm. ^{119}Sn NMR ($CDCl_3$, 112 MHz): δ -104.3 ppm.

$L^{CN}SnAr^*Cl_2$ 24: ^{1}H NMR ($CDCl_3$, 300 MHz): δ 8.24 (d, 1H, H(6), $^{3}J(^{1}H, ^{1}H)$ = 7.5 Hz, $^{3}J(^{119}Sn, ^{1}H) \approx 99$ Hz); 7.49 (d, 2H, *o*-Ph, $^{3}J(^{1}H, ^{1}H)$ = 7.5 Hz, $^{3}J(^{119}Sn, ^{1}H) \approx 96$ Hz); 7.38 (m, 2H, H(4,5)); 7.18 (d, 2H, *m*-Ph, $^{3}J(^{1}H, ^{1}H)$ = 7.5 Hz); 7.14 (d, 1H, H(3), $^{3}J(^{1}H, ^{1}H)$ = 7.5 Hz); 3.62 (s, 2H, CH_2N); 2.53 (t, 2H, α-H, $^{3}J(^{1}H, ^{1}H)$ = 7.5 Hz); 2.11 (s, 6H, NMe_2); 1.51 (m, 2H, β-H); 1.27 (m, 2H, γ-H); 0.84 (t, 3H, δ-H, $^{3}J(^{1}H, ^{1}H)$ = 7.5 Hz) ppm. ^{119}Sn NMR ($CDCl_3$, 112 MHz): δ -170.6 (s) ppm.

$L^{CN}{}_2SnBr_2$ 25: ^{1}H NMR ($CDCl_3$, 300 MHz): δ 8.21 (d, 2H, H(6)); 7.36-7.32 (m, 4H, H(4, 5)); 7.26 (m, 2H, H(3)); 3.31 (s, 4H, CH_2N); 2.22 (m, 12H, NMe_2) ppm. ^{119}Sn NMR ($CDCl_3$, 112 MHz): δ -271.2 ppm.

$L^{CN}SnBr_3$ 26: ^{1}H NMR ($CDCl_3$, 300 MHz): δ 8.05 (d, 1H, H(6)); 7.23 (m, 2H, H(4, 5)); 7.23 (m, 1H, H(3)); 3.81 (s, 2H, CH_2N); 2.52 (m, 6H, NMe_2) ppm. ^{119}Sn NMR ($CDCl_3$, 112 MHz): δ -407 -ppm.

$L^{CN}{}_2SnBuH$ 27: ^{1}H NMR (C_6D_6, 300 MHz): δ 7.74-7.65 (m, 2H, $^{3}J(^{1}H\text{-}^{119/117}Sn)$= 54.1 Hz, H6), 7.17-6.91 (m, 6H, H3-h5), 6.38 (s, 1H, $^{1}J(^{1}H\text{-}^{119}Sn)$= 1980 Hz, $^{1}J(^{1}H\text{-}^{117}Sn)$= 1894 Hz), Sn-H), 3.30-3.13 (m, 4H, N-CH_2), 1.82 (s, 12H, $N(CH_3)_2$), 1.77-1-69 (m, 2H, H9), 1.52-1.36 (q, 2H, H8), 1.37-1.21 (t, 2H, H7), 0.91-0.84 (t, 3H, H10) ppm. ^{13}C NMR (C_6D_6, 75.5 MHz): δ 145.7 ($^{2}J(^{13}C\text{-}^{119/117}Sn)$= 24.1, C2), 143.8 ($^{1}J(^{13}C\text{-}^{119}Sn)$= 539.5 Hz, $^{1}J(^{13}C\text{-}^{117}Sn)$= 517.2 Hz, C1), 138.0 ($^{3}J(^{13}C\text{-}^{119/117}Sn)$= 40.0 Hz,C6), 128.6 ($^{4}J(^{13}C\text{-}^{119/117}Sn)$= 10.3 Hz, C4), 128.2 (couplings under C_6D_6, C3 or C5), 126.9 ($^{3}J(^{13}C\text{-}^{119/117}Sn)$= 52.3 Hz, C3 or C5), 66.3 ($^{3}J(^{13}C\text{-}^{119/117}Sn)$= 21.0 Hz, N-$\underline{C}H_2$), 44.5 (N-($\underline{C}H_3)_2$), 30.7 ($^{3}J(^{13}C\text{-}^{119/117}Sn)$= 17.4 Hz, C9), 27.9

($^{2}J(^{13}C\text{-}^{119/117}Sn)$= 66.9, C8), 14.1 (C10), 12.6 $^{1}J(^{13}C\text{-}^{119}Sn)$= 396.4 Hz, $^{1}J(^{13}C\text{-}^{117}Sn)$= 379.2, C7) ppm. ^{119}Sn NMR (C_6D_6, 112 MHz): -161.9 ($^{1}J(^{119}Sn\text{-}^{1}H)$= 1980 Hz) ppm.

5.11.2 Amine Base Amine Concentration Dependent Dehydrogenative Polymerization

Sn@$^{1\text{ eq. TMEDA}}$*o*-tolyl (RT, 20 min) 12: 4.43 g *o*-tolylSnH$_3$ (20.8 mmol, 2.8 mL), 11 mL Et_2O, 3.1 mL TMEDA (20.8 mmol, 2.42 g, 1 eq.). Anal. Found: C, 27.57; H, 2.42; N, 0.72.

Sn@$^{0.1\text{ eq. TMEDA}}$*o*-tolyl (RT, 45 min) 13: 0.3 g *o*-tolylSnH$_3$ (1.41 mmol, 0.21 mL), 5 mL Et_2O, 0.021 mL TMEDA (0.141 mmol, 0.0164 g, 0.1 eq.). Anal. Found: C, 26.2; H, 2.76; N, 0.97.

5.11.3 Thermally Induced Dehydrocoupling

The aryltin hydride was warmed up to 60°C under vacuum in order to obtain a dark red to brown solid, which was taken up in benzene, filtered and analyzed in the NMR.

H$_2$[(phenyl)Sn-Sn(phenyl)]H$_2$ 11: ^{1}H NMR (C_6D_6, 300 MHz): δ 7.40 (d, 2H, $^{3}J(^{1}H\text{-}^{119/117}Sn)$= 66 Hz, H6), 7.16-7.03 (m, 6H, H3-H5), 5.15 (s, 4H, $^{1}J(^{1}H\text{-}^{119}Sn)$= 1758 Hz, $^{1}J(^{1}H\text{-}^{117}Sn)$= 1677 Hz, $^{2}J(^{1}H\text{-}^{119/117}Sn)$= 138 Hz). ^{119}Sn (^{1}H coupled) NMR (C_6D_6, 112 MHz): -353.9 (tt, $^{1}J(^{119}Sn\text{-}^{1}H)$= 1763 Hz, $^{2}J(^{1}H\text{-}^{119}Sn)$= 150 Hz) ppm.

A 50 mL Schlenk flask equipped with a stirring bar was charged with degassed and dried Et_2O. Subsequently, *o*-tolylSnH$_3$ (**6**) was added using a syringe. The reaction was stirred until the distinct color change to black was achieved. Afterwards, the polymer was separated from the filtrate by using a centrifuge and the resulting filtrate was subjected by GC-MS as well as ^{1}H and ^{119}Sn NMR analysis. The polymeric material was also investigated by EA, SEM, SAXS and WAXS.

Sn@*o*-tolyl (RT, 16 days) 14: 0.3 g *o*-tolylSnH$_3$ (1.41 mmol, 0.21 mL) in 5 mL Et_2O. Anal. Found: C, 17.41; H, 2.09; N, 0.17.

5.11.4 Sonication Assisted Dehydrogenative Polymerization

A 50 mL Schlenk flask was charged with degassed and dried Et_2O and the amine base TMEDA, if used, and placed in the cooled sonication bath. Subsequently, *o*-tolylSnH_3 (**6**) was added using a syringe. The reaction was stirred until the distinct color change to black was achieved. Afterwards, the polymer was separated from the filtrate by using a centrifuge and the resulting filtrate was subjected by GC-MS as well as ^{1}H and ^{119}Sn NMR analysis. The polymeric material was also investigated by EA, SEM, SAXS and WAXS.

Sn@$^{son,\ 1\ eq.\ TMEDA}$*o*-tolyl (RT, 30 min) 15: 0.3 g *o*-tolylSnH_3 (1.41 mmol, 0.21 mL), 5 mL Et_2O, 0.21 mL TMEDA (1,41 mmol, 0.163 g, 1 eq.). Anal. Found: C, 33.2; H, 3.59; N, 2.30.

Sn@^{son}*o*-tolyl (RT, 20 days) 16: 0.3 g *o*-tolylSnH_3 (1.41 mmol, 0.21 mL) in 5 mL Et_2O. Anal. Found: C, 19.56; H, 2.17; N, 0.24.

5.11.5 Dehydrogenative Polymerization Induced by Microwave

A 10 mL microwave vial was charged with degassed and dried DME and the organotin trihydride. Directly after, the reaction mixture was placed in the microwave reactor and the program was started. Afterwards, the polymer was separated from the filtrate by using a centrifuge and the resulting filtrate was subjected by GC-MS as well as ^{1}H and ^{119}Sn NMR analysis. The polymeric material was further investigated by EA, SEM, SAXS and WAXS.

Sn@^{micro}1-naph (100°C, 20 min) 17: 0.3 g 1-naphSnH_3 (1.21 mmol) in 5 mL DME. Anal. Found: C, 57.69; H, 3.57; N, 0.00.

Sn@^{micro}*o*-tolyl (100°C, 20 min) 18: 0.3 g *o*-tolylSnH_3 (1.41 mmol, 0.21 mL) in 5 mL DME.

Sn@^{micro}*o*-tolyl (120°C, 15 min) 19: 0.3 g *o*-tolylSnH_3 (1.41 mmol, 0.21 mL) in 5 mL DME.

5.11.6 Intra-amine Catalysed Dehydrogenation

Numbering of compounds corresponds to the numbering used in the thesis.

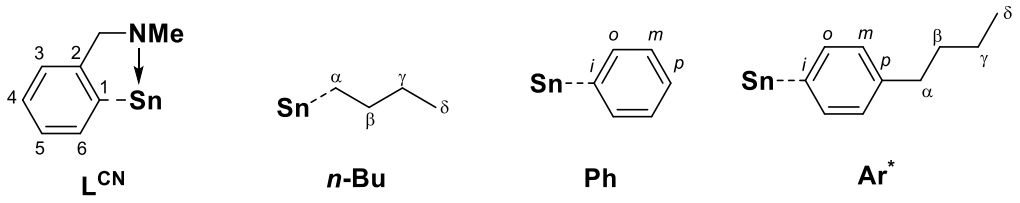

Figure 25: Structural drawings and general NMR numbering of L^{CN}, n-Bu and Ph substituents

5.11.6.1 Preparation of BX_3 Protected C,N-chelated Organotin Halides

A Schlenk tube was charged with a solution of the *C,N*-chelated organotin halide in CH_2Cl_2 and a 1 M BCl_3 solution in hexane was added slowly *via* a syringe while cooling with an ice bath. After complete addition, the bath was removed, the reaction warmed up to room temperature and the reaction stirred overnight. The clear solution was separated from the white precipitation *via* a cannula and the solvent evaporated. The resulting products were subjected in ^{1}H, ^{11}B as well as ^{119}Sn NMR analysis.

$L^{CN}SnPh_2Cl \cdot BCl_3$ 28: 2 g of $L^{CN}SnPh_2Cl$ (4.52 mmol, 1 eq.) were dissolved in 40 mL CH_2Cl_2 and 5 mL of a 1 M BCl_3 solution in hexane (4.97 mmol, 1.1 eq.) were added over 5 minutes while cooling with an ice bath. The reaction mixture turned from clear and colorless into cloudy and bright yellow. After removing the ice bath, the reaction was stirred overnight. The solvent was evaporated and a white solid appeared. For analysis, a small amount was recrystallized from CH_2Cl_2 and hexane to obtain colorless crystals. M.p., 74-75°C. ^{1}H NMR ($CDCl_3$, 300 MHz): δ 7.88 (m, 1H, H(6), $^{3}J(^{119}Sn, ^{1}H)$ = 60 Hz); 7.68 (m, 4H, *o*-Ph); 7.61-7.55 (m, 8H, L^{CN} and Ph moieties); 7.50 (m, 1H, H(3)); 4.67 (s, 2H, CH_2N); 2.71 (m, 6H, NMe_2) ppm. ^{13}C NMR ($CDCl_3$, 75.5 MHz): δ 136.0 (C(2), $^{2}J(^{119/117}Sn, ^{13}C)$ = 50 Hz); 137.2 (*i*-Ph, $^{1}J(^{119/117}Sn, ^{13}C)$ = 626/600 Hz); 139.0 (C(6), $^{2}J(^{119/117}Sn, ^{13}C)$ = 42 Hz); 143.6 (C(1), 136.0 (*o*-Ph, $^{2}J(^{119/117}Sn, ^{13}C)$ = 50 Hz); 131.1 (*p*-Ph), $^{4}J(^{119/117}Sn, ^{13}C)$ = 13 Hz); 130.7 (C(4), $^{4}J(^{119/117}Sn, ^{13}C)$ = 14 Hz); 130.4 C(5); 129.8 (*m*-Ph), $^{3}J(^{119/117}Sn, ^{13}C)$ = 66 Hz); 127.5 (C(3), $^{3}J(^{119/117}Sn, ^{13}C)$ = 62 Hz); 63.3 (CH_2N, $^{n}J(^{119/117}Sn, ^{13}C)$ = 27 Hz); 45.0 (NMe_2) ppm. ^{119}Sn NMR ($CDCl_3$, 112 MHz): δ -48.39 ppm. $^{11}B\{^{1}H\}$ NMR ($CDCl_3$, 96 MHz): δ 9.94 ppm.

$L^{CN}SnBu_2Cl \cdot BCl_3$ 29: 2 g of $L^{CN}SnBu_2Cl$ (4.93 mmol, 1 eq.) were dissolved in 40 mL CH_2Cl_2 and 6 mL of a 1 M BCl_3 solution in hexane (5.96 mmol, 1.1 eq.) were added over 5 minutes while cooling with an ice bath. The reaction mixture turned from a cloudy solution into a clear and bright yellow one. After removing the ice bath, the reaction was stirred overnight. The solvent was evaporated and a colorless oil appeared. ^{1}H NMR ($CDCl_3$, 300 MHz): δ 7.89 (d, 1H, H(6), $^3J(^1H, ^1H)$ = 7 Hz, $^3J(^{119}Sn, ^1H)$ = 57 Hz); 7.56-7.50 (m, 3H, H(3, 4, 5)); 4.59 (s, 2H, CH_2N); 2.81 (m, 6H, NMe_2); 1.68 (br m, 4H, α-CH_2); 1.38 (br, 4H, β-CH_2); 1.38 (sext, 4H, γ-CH_2); 0.91 (t, 6H, δ-CH_3, $^3J(^1H, ^1H)$ = 6 Hz) ppm. $^{13}C\{^1H\}$ NMR ($CDCl_3$, 75.5 MHz): δ 146.9 (C(1), $^1J(^{119/117}Sn, ^{13}C)$ = 412 Hz); 138.1 (C(6), $^2J(^{119/117}Sn, ^{13}C)$ = 31 Hz); 134.9 (C(2)); 133.8 (C(3), $^3J(^{119/117}Sn, ^{13}C)$ = 38 Hz); 130.2 (C(5), $^3J(^{119/117}Sn, ^{13}C)$ = 43 Hz); 130.0 (C(4), $^4J(^{119/117}Sn, ^{13}C)$ = 10 Hz); 64.2 (CH_2N, $^nJ(^{119/117}Sn, ^{13}C)$ = 26 Hz); 45.0 (NMe_2); 27.8 (β-C, $^2J(^{119/117}Sn, ^{13}C)$ = 28 Hz); 26. (γ-C, $^3J(^{119/117}Sn, ^{13}C)$ = 69/55 Hz); 20.0 (α-C, $^1J(^{119/117}Sn, ^{13}C)$ = 384/367 Hz); 13.6 (δ-C) ppm. $^{119}Sn\{^1H\}$ NMR ($CDCl_3$, 112 MHz): δ 86.6 ppm. $^{11}B\{^1H\}$ NMR ($CDCl_2$, 96 MHz): δ 10.3 ppm.

^{1}H NMR (d^8-THF, 300 MHz): δ 7.83 (d, 1H, H(6), $^3J(^1H, ^1H)$ = 7 Hz, $^3J(^{119}Sn, ^1H)$ = 60/46 Hz); 7.62 (d, 1H, H(3), $^3J(^1H, ^1H)$ = 8 Hz, $^4J(^{119}Sn, ^1H)$ = 32 Hz); 7.53-7.49 (m, 3H, H(3, 4, 5)); 4.64 (s, 2H, CH_2N); 2.83 (m, 6H, NMe_2); 1.75 (br m, 4H, α-CH_2); 1.64 (br, 4H, β-CH_2); 1.44 (sext, 4H, γ-CH_2); 0.95 (t, 6H, δ-CH_3) ppm. $^{13}C\{^1H\}$ NMR (d^8-THF, 75.5 MHz): δ 150.5 C(1); 138.7 (C(6), $^2J(^{119/117}Sn, ^{13}C)$ = 30 Hz); 136.1 (C(2)); 135.4 (C(3), $^3J(^{119/117}Sn, ^{13}C)$ = 42 Hz); 130.5 (C(5), $^3J(^{119/117}Sn, ^{13}C)$ = 47 Hz); 130.1 (C(4), $^4J(^{119/117}Sn, ^{13}C)$ = 11 Hz); 65.0 (CH_2N, $^nJ(^{119/117}Sn, ^{13}C)$ = 24 Hz); 45.6 (NMe_2); 29.1 (β-C, $^2J(^{119/117}Sn, ^{13}C)$ = 27 Hz); 27.7 (γ-C, $^3J(^{119/117}Sn, ^{13}C)$ = 84 Hz); 21.1 (α-C, $^1J(^{119/117}Sn, ^{13}C)$ = 432/413 Hz); 14.1 (δ-C) ppm. $^{119}Sn\{^1H\}$ NMR (d^8-THF, 112 MHz): δ 26.6 ppm. $^{11}B\{^1H\}$ NMR (d^8-THF, 96 MHz): δ 10.3 ppm.

$L^{CN}SnPhCl_2 \cdot BCl_3$ 30: 1 g of $L^{CN}SnPhCl_2$ (2.49 mmol, 1 eq.) were dissolved in 40 mL CH_2Cl_2 and 3 mL of a 1 M BCl_3 solution in hexane (2.99 mmol, 1.2 eq.) were added over 5 minutes while cooling with an ice bath. The reaction mixture turned from a clear solution into bright yellow with some white precipitation. After removing the ice bath, the reaction was stirred overnight. The solvent was evaporated and a white solid appeared. ^{1}H NMR ($CDCl_3$, 300 MHz): δ 8.04 (m, 1H, H(6), $^3J(^{119}Sn, ^1H)$ = 80 Hz); 7.71 (m, 4H, *o*-Ph); 7.63-7.56

(m, 8H, L^{CN} and Ph moieties); 4.61 (s, 2H, CH_2N); 2.79 (m, 6H, NMe_2) ppm. $^{119}Sn\{^1H\}$ NMR ($CDCl_3$, 112 MHz): δ -30.7 ppm. $^{11}B\{^1H\}$ NMR ($CDCl_3$, 96 MHz): δ 10.0 ppm.

$L^{CN}SnBuCl_2 \cdot BCl_3$ 31: 1 g of $L^{CN}SnBuCl_2$ (2.63 mmol, 1 eq.) were dissolved in 40 mL CH_2Cl_2 and 3.1 mL of a 1 M BCl_3 solution in hexane (3.1 mmol, 1.2 eq.) were added over 5 minutes while cooling with an ice bath. The reaction mixture turned from a cloudy solution into bright yellow with some white precipitation. After removing the ice bath, the reaction was stirred overnight. The solvent was evaporated and a colorless oil appeared. ^1H NMR ($CDCl_3$, 300 MHz): δ 8.00 (d, 1H, H(6), $^3J(^1H, ^1H)$ = 7 Hz, $^3J(^{119/117}Sn, ^1H)$ = 78/64 Hz); 7.67-7.41 (m, 3H, H(3,4, 5)); 4.57 (s, 2H, CH_2N); 2.89 (m, 6H, NMe_2); 2.20 (br m, 4H, α-CH_2); 1.91 (br, 4H, β-CH_2); 1.47 (m, 4H, γ-CH_2); 0.96 (t, 6H, δ-CH_3) ppm. $^{119}Sn\{^1H\}$ NMR ($CDCl_3$, 112 MHz): δ 26.4 ppm. $^{11}B\{^1H\}$ NMR ($CDCl_3$, 96 MHz): δ 10.2 ppm.

$L^{CN}SnAr^*Cl_2 \cdot BCl_3$ 32: 1 g of $L^{CN}SnAr^*Cl_2$ (2.19 mmol, 1 eq.) were dissolved in 40 mL CH_2Cl_2 and 2.6 mL of a 1 M BCl_3 solution in hexane (2.63 mmol, 1.2 eq.) were added over 5 minutes while cooling with an ice bath. The reaction mixture turned from a clear solution into bright yellow with some white precipitation. After removing the ice bath, the reaction was stirred overnight. The solvent was evaporated and a colorless oil appeared. ^1H NMR ($CDCl_3$, 300 MHz): δ 8.07 (m, 1H, H(6), $^3J(^{119/117}Sn, ^1H)$ = 87/72 Hz); 7.73-7.34 (m, 8H, L^{CN} and Ar^* moieties); 4.70 (s, 2H, CH_2N); 2.79 (m, 6H, NMe_2) 2.67 (br m, 4H, α-CH_2); 1.63 (br, 4H, β-CH_2); 1.38 (m, 4H, γ-CH_2); 0.95 (t, 6H, δ-CH_3) ppm. $^{119}Sn\{^1H\}$ NMR ($CDCl_3$, 112 MHz): δ -262.1 ppm. $^{11}B\{^1H\}$ NMR ($CDCl_3$, 96 MHz): δ 3.2 ppm.

$L^{CN}{}_2SnBr_2 \cdot BBr_3$ 33: 1 g of $L^{CN}{}_2SnBr_2$ (1.83 mmol, 1 eq.) were dissolved in 40 mL CH_2Cl_2 and 3.7 mL of a 1 M BBr_3 solution in hexane (3.66 mmol, 2.1 eq.) were added over 5 minutes while cooling with an ice bath. The reaction mixture turned from a cloudy solution into bright yellow with some white precipitation. After removing the ice bath, the reaction was stirred overnight. The solvent was evaporated and a white solid appeared. ^1H NMR ($CDCl_3$, 300 MHz): δ 8.22 (d, 2H, H(6), $^3J(^1H, ^1H)$ = 7 Hz, $^3J(^{119/117}Sn, ^1H)$ = 92/77 Hz); 7.77-7.69 (m, 4H, H(4, 5)); 7.64 (m, 2H, H(3) $^3J(^{119}Sn, ^1H)$ = 48/36 Hz); 4.71 (s, 4H, CH_2N); 3.07 (m, 12H, NMe_2) ppm. $^{119}Sn\{^1H\}$ NMR ($CDCl_3$, 112 MHz): δ -81.6 ppm. $^{11}B\{^1H\}$ NMR ($CDCl_3$, 96 MHz): δ 3.5 ppm.

$L^{CN}SnBr_3 \cdot BBr_3$ 34: 1 g of $L^{CN}SnBr_3$ (2.03 mmol, 1 eq.) were dissolved in 40 mL CH_2Cl_2 and 2.4 mL of a 1 M BBr_3 solution in hexane (2.44 mmol, 1.2 eq.) were added over 5 minutes while cooling with an ice bath. The reaction mixture turned from a cloudy solution into bright yellow with some white precipitation. After removing the ice bath, the reaction was stirred overnight. The solvent was evaporated and a white solid appeared. For analysis a small amount was recrystallized from CH_2Cl_2 and hexane to obtain colorless crystals. M.p., 163-164 °C. ^{1}H NMR ($CDCl_3$, 300 MHz): δ 7.93 (d, 1H, H(6), $^3J(^1H, ^1H)$ = 7 Hz, $^3J(^{119/117}Sn, ^1H)$ = 126/111 Hz); 7.80-7.70 (m, 2H, H(4, 5)); 7.63 (m, 1H, H(3) $^3J(^{119}Sn, ^1H)$ = 72/50 Hz); 5.15 (s, 2H, CH_2N); 3.08 (m, 6H, NMe_2) ppm. $^{13}C\{^1H\}$ NMR ($CDCl_3$, 75.5 MHz): δ 142.1 (C(1)); 136.7 (C(6), $^2J(^{119/117}Sn, ^{13}C)$ = 88 Hz); 134.5 (C(2)); 132.9 (C(3), $^3J(^{119/117}Sn, ^{13}C)$ = 22 Hz); 131.5 (C(5), $^3J(^{119/117}Sn, ^{13}C)$ = 106 Hz); 130.0 (C(4)); 63.1 (CH_2N, $^nJ(^{119/117}Sn, ^{13}C)$ = 42 Hz); 46.7 (NMe_2) ppm. $^{119}Sn\{^1H\}$ NMR ($CDCl_3$, 112 MHz): δ -257.9 ppm. $^{11}B\{^1H\}$ NMR ($CDCl_3$, 96 MHz): δ 3.2 ppm.

5.11.6.2 Conversion of $L^{CN}SnBu_2Cl \cdot BCl_3$ to the Corresponding Hydride

A Schlenk tube was charged with a solution of the C,N-chelated organotin halide in CH_2Cl_2 and a 1 M solution of $K(BEt_3)H$ in THF was added slowly *via* a syringe while cooling with an ice bath. After complete addition, the bath was removed, the reaction warmed up to room temperature and the reaction stirred overnight. The cloudy solution was filtered *via* a cannula and the solvent evaporated. The resulting products were subjected in ^{1}H, ^{11}B as well as ^{119}Sn NMR analysis.

$L^{CN}SnBu_2H \cdot BCl_3$ 27: 1.2 g of $L^{CN}SnBu_2H \cdot BCl_3$ (2.21 mmol, 1 eq.) were dissolved in 30 mL THF and 2.2 mL of a 1 M $K(BEt_3)H$ solution in THF (2.21mmol, 1 eq) were added over 5 minutes while cooling with an ice bath. The solvent was evaporated and a colorless oil appeared. ^{1}H NMR (d^8-THF, 300 MHz): δ 7.83 (d, 1H, H(6), $^3J(^1H, ^1H)$ = 7 Hz, $^3J(^{119/117}Sn, ^1H)$ = 56/55 Hz); 7.67-7.58 (m, 2H, H(4, 5)); 7.42 (d, 1H, H(3), $^3J(^1H, ^1H)$ = 7 Hz); 5.82 (s, 1H, $^1J(^1H\text{-}^{119}Sn)$= 1720 Hz) 4.66 (s, 2H, CH_2N); 2.80-2.81 (m, 6H, NMe_2); 1.58 (br m, 4H, α-CH_2); 1.35 (br, 4H, α-CH_2); 1.26 (m, 4H, γ-CH_2); 0.89 (t, 6H, δ-CH_3, $^3J(^1H, ^1H)$ = 6 Hz) ppm. $^{13}C\{^1H\}$NMR (d^8-THF, 75.5 MHz): δ 147.7 (C(1), $^1J(^{119/117}Sn, ^{13}C)$ = 397/380 Hz); 139.2 (C(6), $^2J(^{119/117}Sn, ^{13}C)$ = 32 Hz); 137.5 (C(2)); 135.1 (C(3), $^3J(^{119/117}Sn, ^{13}C)$ = 31 Hz); 130.1 (C(5), $^3J(^{119/117}Sn, ^{13}C)$ = 42 Hz); 129.6 (C(4), $^4J(^{119/117}Sn, ^{13}C)$ = 10 Hz); 64.9 (CH_2N, $^nJ(^{119/117}Sn, ^{13}C)$ = 22 Hz); 45.1 (NMe_2); 30.1 (β-C, $^2J(^{119/117}Sn, ^{13}C)$ = 22 Hz); 28.0 (γ-C,

$^{3}J(^{119/117}Sn, ^{13}C)$ = 62 Hz); 14.1 (δ-C); 11.2 (α-C, $^{1}J(^{119/117}Sn, ^{13}C)$ = 370/360 Hz) ppm. $^{119}Sn\{^{1}H\}$ NMR (d^{8}-THF, 112 MHz): δ -118.4 ppm. ^{119}Sn NMR (d^{8}-THF, 112 MHz): δ -118.6 (d, $^{1}J(^{119/117}Sn, ^{13}C)$ = 1720 Hz) ppm. $^{11}B\{^{1}H\}$ NMR (d^{8}-THF, 96 MHz): δ 10.3 ppm.

5.11.6.3 Conversion of $L^{CN}SnBr_3 \cdot BBr_3$ *via* the Corresponding Hydrides Towards Sn@L^{CN}

1 g of $L^{CN}SnBr_3$ (2.03 mmol, 1 eq.) were dissolved in 40 mL CH_2Cl_2 and 2.4 mL of a 1 M BBr_3 solution in hexane (2.44 mmol, 1.2 eq.) were added over 5 minutes while cooling with an ice bath. The reaction mixture turned from a cloudy solution into bright yellow with some white precipitation. After removing the ice bath, the reaction was stirred overnight. The solvent was evaporated and a white solid appeared. The product was dissolved in 30 mL THF and 5.3 mL of a 1 M $K(BEt_3)H$ solution in THF (5.24 mmol, 3 eq.) were added slowly while cooling with an ethanol/N_2 bath (-40°C). Within adding the first half of the reduction agent, the reaction mixture turned yellow, but after stirring for 1 minute, the color disappeared and a cloudy solution was observed. After adding the second portion of $K(BEt_3)H$, the reaction mixture started to turn yellow. Within 1 hour the color change from yellow, over orange, to dark red and the production of hydrogen could be observed. After stirring overnight, a brown to black precipitate could be obtained. The product was investigated *via* SEM, SAXS, WAXS and EA.

5.11.6.4 Crystallographic Data

Table 3: Crystallographic data

Compound	$L^{CN}SnPh_2Cl \cdot BCl_3*CH_2Cl_2$ (**28**)	$L^{CN}SnBr_3 \cdot BBr_3$ (**34**)	$[(L^{CN})_2SnCl_3]^+ \cdot ½ [SnCl_6]^{2-}$ (**36**)
Empirical formula	$C_{22}H_{24}BCl6NSn$	$C_9H_{12}BBr_6NSn$	$C_{38}H_{56}Cl_{16}N_4Sn_3$
Crystal system	triclinic	monoclinic	triclinic
Formula weight	644.62	743.16	1492.13
Space group	P -1	P 2_1/n	P -1
a (Å)	8.6372(5)	10.7295(10)	8.0253(9)
b (Å)	10.1406(6)	15.2791(14)	13.7472(18)
c (Å)	15.6729(9)	10.8016(8)	14.8487(18)
α (°)	91.024(3)	90	116.520(4)
β (°)	103.514(2)	92.872(3)	95.452(5)
γ (°)	102.184(2)	90	98.792(4)
Z	2	4	1
V (Å^3)	2039.9(3)	1768.6(3)	1423.7(3)
D_c/g cm^{-3}	1.645	2.791	1.740
Crystal size (mm)	0.32 x 0.19 x 0.15	0.20 x 0.20 x 0.18	0.19 x 0.12 x 0.06
Crystal shape	block	block	block
Crystal color	colorless	colorless	colorless
μ (mm^{-1})	1.609	14.983	2.088
F(000)	640	1352	734
h; k; l range	-11,11; -13,13; -20,20	-13, 13; -19,19; -14,12	-10,10; -17,17; -19,19
θ range/°	2.377 - 27.624	2.311 - 27.614	2.613 - 27.588
Reflections measured	36036	40360	42103
- independent (R_{int}) [a]	6053	4098	6579
- observed [I>2σ(I)]	5356	2848	5760
Parameters refined	282	165	290
Max/min τ/eÅ^{-3}			
GOF [b]	1.052	1.033	1.101
R / wR [c]	0.0348 / 0.0795	0.0549 / 0.0939	0.0220 / 0.0452

[a] $R_{int} = \Sigma \left| F_o^2 - F_{o,mean}^2 \right| / \Sigma F_o^2$, [b] $S = [\Sigma(w(F_o^2 - F_c^2)^2)/(N_{diffrs} - N_{params})]^{½}$, [c] Weighting scheme: $w = [\sigma^2(F_o^2) + (w_1P)^2 + w_2P]^{-1}$, where $P = [\max(F_o^2) + 2F_c^2]$, $R(F) = \Sigma \left| \left| F_o \right| - \left| F_c \right| \right| / \Sigma \left| F_o \right|$, $wR(F^2) = [\Sigma(w(F_o^2 - F_c^2)^2)/(\Sigma w(F_o^2)^2)]^{½}$

Table 4: Bond lengths of the crystal structures

Compound	Sn – C_{Ph} (Å) avg.	Sn – C_{LCN} (Å) avg.	Sn – X (Å) X=Cl/Br avg.	N - B (Å)
$L^{CN}SnPh_2Cl \cdot BCl_3*CH_2Cl_2$ (**28**)	2.116 (3)	2.144 (3)	2.339 (1)	1.636 (4)
$L^{CN}SnBr_3 \cdot BBr_3$ (**34**)	-	2.123 (9)	2.421 (1)	1.617 (13)
$[(L^{CN})_2SnCl_3]^+ \cdot ½ [SnCl_6]^{2-}$ (**36**)	-	2.139 (2)	2.481 (6)	-

Table 5: Angles of the crystal structures

Compound	C_{Ph} – Sn – C_{Ph} (°)	C_{Ph} – Sn – C_{LCN} (°)	C_{Ph} – Sn – X (°) X=Cl/Br	C_{LCN} – Sn – X (°) X=Cl/Br avg.	C_{LCN} – N – B (°)
$L^{CN}SnPh_2Cl \cdot BCl_3*CH_2Cl_2$ (**28**)	115.19 (12)	116.87(11) 108.27 (11)	105.03 (9) 101.95 (9)	108.19 (8)	109.2 (2)
$L^{CN}SnBr_3 \cdot BBr_3$ (**34**)	-	122.3 (2)	-	122.3 (2)	109.3 (3)
$[(L^{CN})_2SnCl_3]^+ \cdot ½ [SnCl_6]^{2-}$ (**36**)	-	-	-	123.56 (8)	-

6 References

1. Zeppek, C. Amine Base Induced Polymerization of Aryltin Hydrides: Mechanistic Insights & Nanomaterial Characterization. Doctoral Thesis, Graz University of Technology, Graz, Austria, 2015.
2. Zeppek, C.; Torvisco, A.; Flock, M.; Guglieri, C.; Amenitsch, H.; Uhlig, F., *J. Mater. Chem.* ***in prep.***
3. Foucher, D., Catenated Germanium and Tin Oligomers and Polymers. In *Main Group Strategies towards Functional Hybrid Materials*, Baumgartner, T.; Jäkle, F., Eds. Wiley: pp 209-236.
4. von Frankland, E., *Justus Liebigs Annalen der Chemie* **1849,** *71*(2), 171-213.
5. von Frankland, E., *Justus Liebigs Annalen der Chemie* **1849,** *71*(2), 213-216.
6. Grignard, V. Theses sur les combinaisons organo-magnesienes mixtes et leur application a des syntheses. University of Lyon, 1901.
7. Ingham, R. K.; Rosenberg, S. D.; Gilman, H., *Chem. Rev.* **1960,** *60*(5), 459-539.
8. Edgell, W. F.; Ward, C. H., *J. Am. Chem. Soc.* **1954,** *76*(4), 1169-1169.
9. Foldesi, I., *Acta Chim. Acad. Sci. Hung.* **1965,** *45*(3), 237-244.
10. van der Kerk, G. J. M.; Luijten, J. G. A., *Journal of Applied Chemistry* **1956,** *6*(2), 56-60.
11. Bogdanovic, B.; Bons, P.; Konstantinovic, S.; Schwickardi, M.; Westeppe, U., *Chem. Ber.* **1993,** *126*(6), 1371-1383.
12. Clark, H. C.; Willis, C. J., *J. Am. Chem. Soc.* **1960,** *82*(8), 1888-1891.
13. Kocheshkov, K. A., *Ber. Dtsch. Chem. Ges. B* **1933,** *66B*, 1661-1665.
14. Kocheshkov, K. A.; Nadi, M. M., *Ber. Dtsch. Chem. Ges. B* **1934,** *67B*, 717-721.
15. Kocheshkov, K. A.; Nesmeyanov, A. N., *Ber. Dtsch. Chem. Ges. B* **1931,** *64B*, 628-636.
16. Kozeshkov, K. A., *Ber. Dtsch. Chem. Ges. B* **1929,** *62B*, 996-999.
17. Abraham, M. H.; Hill, J. A., *J. Organomet. Chem.* **1967,** *7*(1), 11-21.
18. Voronkov, M. G.; Abzaeva, K. A., Genesis and Evolution in the Chemistry of Organogermanium, Organotin and Organolead Compounds. In *The Chemistry of Organic Germanium, Tin and Lead Compounds*, John Wiley & Sons, Ltd: 2003; pp 1-130.
19. Paneth, F., *Ber. Dtsch. Chem. Ges. B* **1920,** *53B*, 1710-1717.
20. Kraus, C. A.; Greer, W. N., *J. Am. Chem. Soc.* **1922,** *44*, 2629-2633.
21. Wittig, G.; Meyer, F. J.; Lange, G., *Justus Liebigs Ann. Chem.* **1951,** *571*, 167-201.
22. Bullard, R. H.; Vinger, R. A., *J. Am. Chem. Soc.* **1929,** *51*, 892-894.
23. Chambers, R. F.; Scherer, P. C., *J. Am. Chem. Soc.* **1926,** *48*, 1054-1062.
24. Finholt, A. E.; Bond, A. C.; Schlesinger, H. I., *J. Am. Chem. Soc.* **1947,** *69*(5), 1199-1203.
25. Zeppek, C.; Fischer, R. C.; Torvisco, A.; Uhlig, F., *Can. J. Chem.* **2014,** *92*(6), 556-564.
26. Zeppek, C.; Pichler, J.; Torvisco, A.; Flock, M.; Uhlig, F., *J. Organomet. Chem.* **2013,** *740*, 41-49.
27. Adams, S.; Draeger, M., *Main Group Met. Chem.* **1988,** *11*(3), 151-180.
28. Carraher, C. E., Jr.; Pittman, C. U., Jr.; Zeldin, M.; Abd-El-Aziz, A. S., *Macromol. Containing Met. Met.-Like Elem.* **2005,** *4*(Group IVA Polymers), 225-261.
29. Caseri, W., *Chem. Soc. Rev.* **2016,** *45*(19), 5187-5199.
30. Choffat, F.; Smith, P.; Caseri, W., *Adv. Mater.* **2008,** *20*(11), 2225-2229.
31. Davies, A. G., Organotin Hydrides. In *Organotin Chemistry*, Wiley-VCH Verlag GmbH & Co. KGaA: 2004; pp 244-265.
32. Harrypersad, S.; Foucher, D., *Chem. Commun.* **2015,** *51*(33), 7120-7123.

33. Jurkschat, K.; Mehring, M. In *Organometallic polymers of germanium, tin and lead*, 2002; John Wiley & Sons Ltd.: 2002; pp 1543-1651.
34. Manners, I., *Angewandte Chemie International Edition in English* **1996,** *35*(15), 1602-1621.
35. Manners, I., Polymers with Metal-Metal Bonds in the Main Chain. In *Synthetic Metal-Containing Polymers*, Wiley-VCH Verlag GmbH & Co. KGaA: 2004; pp 181-202.
36. Sharma, H. K.; Pannell, K. H., Organotin polymers and related materials. In Davies, A. G.; Gielen, M.; Pannell, K. H.; Tiekink, E. R. T., Eds. John Wiley & Sons Ltd.: 2008; pp 376-391.
37. Sita, L. R., *Acc. Chem. Res.* **1994,** *27*(7), 191-197.
38. Sita, L. R., *Adv. Organomet. Chem.* **1995,** *38*, 189-243.
39. Trummer, M.; Choffat, F.; Smith, P.; Caseri, W., *Macromol. Rapid Commun.* **2012,** *33*(6-7), 448-460.
40. Watanabe, A., Ge- and Sn-Containing Polymers. In *Encyclopedia of Polymeric Nanomaterials*, Kobayashi, S.; Müllen, K., Eds. Springer Berlin Heidelberg: Berlin, Heidelberg, 2014; pp 1-10.
41. Harrypersad, S.; Liao, L.; Khan, A.; Wylie, R. S.; Foucher, D., *Journal of Inorganic and Organometallic Polymers and Materials* **2015,** *25*(3), 515-528.
42. Lu, V.; Tilley, T. D., *Macromolecules* **1996,** *29*(17), 5763-5764.
43. Sita, L. R., *Organometallics* **1992,** *11*(4), 1442-1444.
44. Sita, L. R.; Terry, K. W.; Shibata, K., *J. Am. Chem. Soc.* **1995,** *117*(30), 8049-8050.
45. Babcock, J. R.; Sita, L. R., *J. Am. Chem. Soc.* **1996,** *118*(49), 12481-12482.
46. Devylder, N.; Hill, M.; Molloy, K. C.; Price, G. J., *Chem. Commun.* **1996,** (6), 711-712.
47. Haeberle, K.; Draeger, M., *Z. Naturforsch., B: Chem. Sci.* **1987,** *42*(3), 323-329.
48. Imori, T.; Lu, V.; Cai, H.; Tilley, T. D., *J. Am. Chem. Soc.* **1995,** *117*(40), 9931-9940.
49. Imori, T.; Tilley, T. D., *J. Chem. Soc., Chem. Commun.* **1993,** (21), 1607-1609.
50. Lu, V. Y.; Tilley, T. D., *Macromolecules* **2000,** *33*(7), 2403-2412.
51. Neale, N. R.; Tilley, T. D., *Tetrahedron* **2004,** *60*(34), 7247-7260.
52. Okano, M.; Matsumoto, N.; Arakawa, M.; Tsuruta, T.; Hamano, H., *Chem. Commun.* **1998,** (17), 1799-1800.
53. Tilley, T. D.; Imori, T. High molecular weight polystannanes by metal-catalyzed dehydropolymerization. US5488091A, 1996.
54. Trummer, M.; Solenthaler, D.; Smith, P.; Caseri, W., *RSC Adv.* **2011,** *1*(5), 823-833.
55. Trummer, M.; Zemp, J.; Sax, C.; Smith, P.; Caseri, W., *J. Organomet. Chem.* **2011,** *696*(19), 3041-3049.
56. Zou, W. K.; Yang, N. L., *Polym. Prepr. (Am. Chem. Soc., Div. Polym. Chem.)* **1992,** *33*(2), 188-189.
57. Choffat, F.; Buchmueller, Y.; Mensing, C.; Smith, P.; Caseri, W., *J. Inorg. Organomet. Polym. Mater.* **2009,** *19*(2), 166-175.
58. de Lima, G. M.; Toupance, T.; Arkis, E.; Chaniotakis, N.; Cusack, P. A.; Lacroix, P. G.; Farfán, N.; Jousseaume, B.; Sharma, H. K.; Pannell, K. H.; Haiduc, I.; Tiekink, E. R. T.; Zukerman-Schpector, J., Materials Chemistry and Structural Chemistry of Tin Compounds. In *Tin Chemistry*, John Wiley & Sons, Ltd: 2008; pp 285-411.
59. Harada, T., *Sci. Pap. Inst. Phys. Chem. Res. (Jpn.)* **1939,** *35*, 290-329.
60. Skotheim, T. A., *Handbook of Conducting Polymers, Second Edition*. CRC Press: New York, 1997; p 1120.

61. Carraher, C. E.; Currell, B.; Pittman, C.; Sheats, J.; Zeldin, M., *Inorganic and Metal-Containing Polymeric Materials*. Springer US: 2012.
62. Mallela, S. P.; Saar, Y.; Hill, S.; Geanangel, R. A., *Inorg. Chem.* **1999,** *38*(12), 2957-2960.
63. Deacon, P. R.; Devylder, N.; Hill, M. S.; Mahon, M. F.; Molloy, K. C.; Price, G. J., *J. Organomet. Chem.* **2003,** *687*(1), 46-56.
64. Colton, R.; Dakternieks, D., *Inorg. Chim. Acta* **1988,** *143*(2), 151-159.
65. Löwig, C., *Journal für Praktische Chemie* **1852,** *57*(1), 385-434.
66. Cahours, A., *Compt. rend. 88*, 725-727.
67. Cahours, A.; Demarcay, E., *Compt. rend. 88*, 1112-1117.
68. Pfeiffer, P., *Ber. Dtsch. Chem. Ges.* **1911,** *44*, 1269-1274.
69. Mustafa, A.; Achilleos, M.; Ruiz-Iban, J.; Davies, J.; Benfield, R. E.; Jones, R. G.; Grandjean, D.; Holder, S. J., *React. Funct. Polym.* **2006,** *66*(1), 123-135.
70. Priestley, R.; Walser, A. D.; Dorsinville, R.; Zou, W. K.; Xu, D. Y.; Yang, N. L., *Opt. Commun.* **1996,** *131*(4,5,6), 347-350.
71. Holder, S. J.; Jones, R. G.; Benfield, R. E.; Went, M. J., *Polymer* **1996,** *37*(15), 3477-3479.
72. Khan, A.; Gossage, R. A.; Foucher, D. A., *Can. J. Chem.* **2010,** *88*(10), 1046-1052.
73. Neale, N. R.; Tilley, T. D., *J. Am. Chem. Soc.* **2002,** *124*(15), 3802-3803.
74. Thompson, S. M.; Schubert, U., *Inorg. Chim. Acta* **2003,** *350*, 329-338.
75. Thompson, S. M.; Schubert, U., *Inorg. Chim. Acta* **2004,** *357*(6), 1959-1964.
76. Choffat, F.; Käser, S.; Wolfer, P.; Schmid, D.; Mezzenga, R.; Smith, P.; Caseri, W., *Macromolecules* **2007,** *40*(22), 7878-7889.
77. Choffat, F.; Smith, P.; Caseri, W., *J. Mater. Chem.* **2005,** *15*(18), 1789-1792.
78. Bukalov, S. S.; Leites, L. A.; Lu, V.; Tilley, T. D., *Macromolecules* **2002,** *35*(5), 1757-1761.
79. Woo, H.-G.; Park, J.-M.; Song, S.-J.; Yang, S.-Y.; Kim, I.-S.; Kim, W.-G., *Bull. Korean Chem. Soc.* **1997,** *18*(12), 1291-1295.
80. Woo, H.-G.; Song, S.-J.; Kim, B.-H., *Bull. Korean Chem. Soc.* **1998,** *19*(11), 1161-1164.
81. Schittelkopf, K.; Fischer, R. C.; Meyer, S.; Wilfling, P.; Uhlig, F., *Appl. Organomet. Chem.* **2010,** *24*(12), 897-901.
82. Aitken, C.; Harrod, J. F.; Malek, A.; Samuel, E., *J. Organomet. Chem.* **1988,** *349*(3), 285-291.
83. Beckmann, J.; Duthie, A.; Grassmann, M.; Semisch, A., *Organometallics* **2008,** *27*(7), 1495-1500.
84. Khan, A.; Komejan, S.; Patel, A.; Lombardi, C.; Lough, A. J.; Foucher, D. A., *J. Organomet. Chem.* **2015,** *776*(0), 180-191.
85. Khan, A.; Lough, A. J.; Gossage, R. A.; Foucher, D. A., *Dalton Trans.* **2013,** *42*(7), 2469-2476.
86. Ward, J.; Al-Alul, S.; Forbes, M. W.; Burrow, T. E.; Foucher, D. A., *Organometallics* **2013,** *32*(10), 2893-2901.
87. Sommer, R.; Neumann, W. P.; Schneider, B., *Tetrahedron Lett.* **1964,** *5*(51), 3875-3878.
88. Costisella, B.; Englich, U.; Prass, I.; Schürmann, M.; Ruhlandt-Senge, K.; Uhlig, F., *Organometallics* **2000,** *19*(13), 2546-2550.
89. Okano, M.; Watanabe, K., *Electrochem. Commun.* **2000,** *2*(7), 471-474.
90. Neumann, W. P.; Koenig, K., *Angew. Chem.* **1962,** *74*, 215.
91. Neumann, W. P.; Koenig, K., *Justus Liebigs Ann. Chem.* **1964,** *677*, 1-11.
92. Davies, A. G.; Osei-Kissi, D. K., *J. Organomet. Chem.* **1994,** *474*(1-2), C8-C10.
93. Mathiasch, B., *Inorg. Nucl. Chem. Lett.* **1977,** *13*(1), 13-15.

94. Neumann, W. P., *The Organic Chemistry of Tin*. Interscience: 1970.
95. Poller, R. C., *The chemistry of organotin compounds*. Logos P.: 1970.
96. Lechner, M.-L.; Trummer, M.; Bräunlich, I.; Smith, P.; Caseri, W.; Uhlig, F., *Appl. Organomet. Chem.* **2011,** *25*(10), 769-776.
97. Sindlinger, C. P.; Stasch, A.; Bettinger, H. F.; Wesemann, L., *Chem. Sci.* **2015,** *6*, 4737-4751.
98. Sindlinger, C. P.; Wesemann, L., *Chem. Sci.* **2014,** *5*(7), 2739-2746.
99. Neumann, W. P.; Pedain, J.; Sommer, R., *Justus Liebigs Ann. Chem.* **1966,** *694*, 9-18.
100. Pichler, J.; Torvisco, A.; Bottke, P.; Wilkening, M.; Uhlig, F., *Can. J. Chem.* **2014,** *92*(6), 565-573.
101. Finholt, A. E.; Bond, A. C., Jr.; Wilzbach, K. E.; Schlesinger, H. I., *J. Am. Chem. Soc.* **1947,** *69*, 2692-2696.
102. Emeleus, H. J.; Kettle, S. F. A., *J. Chem. Soc.* **1958**, 2444-2448.
103. Suslick, K. S.; Hyeon, T.; Fang, M., *Chemistry of Materials* **1996,** *8*(8), 2172-2179.
104. Suslick, K. S.; Price, G. J., *Annual Review of Materials Science* **1999,** *29*(1), 295-326.
105. Brédas, J. L.; Silbey, R., *Conjugated Polymers: The Novel Science and Technology of Highly Conducting and Nonlinear Optically Active Materials*. Springer Netherlands: 2012.
106. Choffat, F.; Wolfer, P.; Smith, P.; Caseri, W., *Macromol. Mater. Eng.* **2010,** *295*(3), 210-221.
107. Nöth, H.; Vahrenkamp, H., *Chemische Berichte* **1966,** *99*(3), 1049-1067.
108. Holeček, J.; Nádvorník, M.; Handlíř, K.; Lyčka, A., *Journal of Organometallic Chemistry* **1983,** *241*(2), 177-184.
109. Armand, M.; Tarascon, J. M., *Nature* **2008,** *451*(7179), 652-657.
110. Tarascon, J. M.; Armand, M., *Nature* **2001,** *414*(6861), 359-367.
111. Hu, R.; Zhu, M.; Wang, H.; Liu, J.; Liuzhang, O.; Zou, J., *Acta Mater.* **2012,** *60*(12), 4695-4703.
112. Kravchyk, K.; Protesescu, L.; Bodnarchuk, M. I.; Krumeich, F.; Yarema, M.; Walter, M.; Guntlin, C.; Kovalenko, M. V., *J. Am. Chem. Soc.* **2013,** *135*(11), 4199-4202.
113. Wang, B.; Luo, B.; Li, X.; Zhi, L., *Mater. Today* **2012,** *15*(12), 544-552.
114. Goodenough, J. B.; Kim, Y., *Chem. Mater.* **2010,** *22*(3), 587-603.
115. Xu, L.; Kim, C.; Shukla, A. K.; Dong, A.; Mattox, T. M.; Milliron, D. J.; Cabana, J., *Nano Lett.* **2013,** *13*(4), 1800-1805.
116. Biedermann, J. Synthesis and electrochemical studies of aryl subsituted Group 14 compounds. Doctoral Thesis, Graz University of Technology, Graz, Austria, 2018.
117. Friedmann, D.; Hakki, A.; Kim, H.; Choi, W.; Bahnemann, D., *Green Chemistry* **2016,** *18*(20), 5391-5411.
118. Altomare, A.; Cascarano, G.; Giacovazzo, C.; Guagliardi, A., *J. Appl. Crystallogr.* **1993,** *26*(3), 343-350.
119. Sheldrick, G. M., *Acta Crystallographica. Section C, Structural Chemistry* **2015,** *71*(Pt 1), 3-8.